JNeurosci
THE JOURNAL OF NEUROSCIENCE

Research Report: Regular Manuscript

Depolarization-dependent C-Raf signaling promotes hyperexcitability and reduces opioid sensitivity of isolated nociceptors after spinal cord injury

https://doi.org/10.1523/JNEUROSCI.0810-20.2020

Cite as: J. Neurosci 2020; 10.1523/JNEUROSCI.0810-20.2020

Received: 7 April 2020
Revised: 16 June 2020
Accepted: 13 July 2020

Depolarization-dependent C-Raf signaling promotes hyperexcitability and reduces opioid sensitivity of isolated nociceptors after spinal cord injury

Abbreviated title: Depolarization and SCI reduce opioid sensitivity

Anibal Garza Carbajal[1], Alexis Bavencoffe[1], Edgar T. Walters[1], and Carmen W. Dessauer[1,*]

[1]Department of Integrative Biology and Pharmacology, McGovern Medical School at UT Health, Houston, Texas 77030

* Corresponding author:
Dr. Carmen W. Dessauer
Department of Integrative Biology and Pharmacology
McGovern Medical School
University of Texas Health Science Center, Houston, TX 77030
Phone: 713-500-6308
Email: Carmen.W.Dessauer@uth.tmc.edu

Number of pages:	39
Number of Figures:	8
Number of Tables:	1
Number of words:	
Abstract:	250
Significance Statement:	120
Introduction:	639
Discussion:	1496

Conflict of Interest: The authors declare no competing financial interests.

Acknowledgements: We thank Emily Spence and Max Odem for rat SCI surgeries and Erica Lee for help with pRKIP analysis. This work was supported by National Institute of Neurological Diseases and Stroke Grant NS091759 to C.W.D. and E.T.W. and grant #545880 from the Craig H. Neilsen Foundation to C.W.D.

Abstract

Chronic pain caused by spinal cord injury (SCI) is notoriously resistant to treatment, particularly by opioids. After SCI, dorsal root ganglion neurons show hyperactivity and chronic depolarization of resting membrane potential (RMP) that is maintained by cAMP signaling through PKA and EPAC. Importantly, SCI also reduces the negative regulation by Gαi of adenylyl cyclase and its production of cAMP, independent of alterations in G protein-coupled receptors and/or G proteins. Opioid reduction of pain depends upon coupling of opioid receptors to Gαi/o family members. Combining high-content imaging and cluster analysis, we show that in male rats SCI decreases opioid responsiveness in vitro within a specific subset of small-diameter nociceptors that bind isolectin B4. This SCI effect is mimicked in nociceptors from naïve animals by a modest 5 min depolarization of RMP (15 mM K^+; -45 mV), reducing inhibition of cAMP signaling by mu-opioid receptor agonists DAMGO and morphine. Disinhibition and activation of C-Raf by depolarization-dependent phosphorylation are central to these effects. Expression of an activated C-Raf reduces sensitivity of adenylyl cyclase to opioids in non-excitable HEK293 cells, while inhibition of C-Raf or treatment with the hyperpolarizing drug retigabine restores opioid responsiveness and blocks spontaneous activity of nociceptors after SCI. Inhibition of ERK downstream of C-Raf also blocks SCI-induced hyperexcitability and depolarization, without direct effects on opioid responsiveness. Thus, depolarization-dependent C-Raf and downstream ERK activity maintain a depolarized resting membrane potential and nociceptor hyperactivity after SCI, providing a self-reinforcing mechanism to persistently promote nociceptor hyperexcitability and limit the therapeutic effectiveness of opioids.

58 **Significance Statement**

59 Chronic pain induced by spinal cord injury (SCI) is often permanent and debilitating, and usually
60 refractory to treatment with analgesics, including opioids. SCI-induced pain in a rat model has
61 been shown to depend upon persistent hyperactivity in primary nociceptors (injury-detecting
62 sensory neurons), associated with a decrease in the sensitivity of adenylyl cyclase production of
63 cAMP to inhibitory Gαi proteins in dorsal root ganglia. This study shows that SCI and one
64 consequence of SCI — chronic depolarization of resting membrane potential — decrease
65 sensitivity to opioid-mediated inhibition of cAMP and promote hyperactivity of nociceptors by
66 enhancing C-Raf activity. ERK activation downstream of C-Raf is necessary for maintaining
67 ongoing depolarization and hyperactivity, demonstrating an unexpected positive feedback loop
68 to persistently promote pain.

69

70 **Introduction**

71 A highly distressing and often permanent complication of traumatic spinal cord injury (SCI) is
72 chronic pain (Widerstrom-Noga, 2017). Like many forms of chronic pain, SCI-induced pain is
73 often refractory to treatment by available pain medications, including opioids (Bryce, 2018).
74 While alterations within the damaged spinal cord as well as the brain contribute to chronic SCI
75 pain (Kramer et al., 2017; Vierck, 2019), our group and others have shown that electrical activity
76 generated in peripheral terminals and cell bodies of sensory neurons located in dorsal root
77 ganglia (DRGs) persistently increases after SCI (Carlton et al., 2009; Bedi et al., 2010; Ritter et
78 al., 2015; Odem et al., 2018). Mechanisms of hyperactivity in nociceptors are logical targets for
79 ameliorating chronic SCI pain because Nav1.8 expression (characteristic of most nociceptors
80 and important for their action potential generation) was found to be necessary for chronic SCI
81 pain in rats as measured by reflexive and operant behavioral tests (Yang et al., 2014).

82 We have previously shown that cAMP signaling is required for maintaining persistent
83 hyperexcitable alterations induced by SCI in nociceptors (Bavencoffe et al., 2016; Berkey et al.,
84 2020). Unexpectedly, the negative regulation of cAMP production at the level of adenylyl
85 cyclase (AC) by Gαi proteins was reduced after SCI in membrane preparations from DRGs,
86 independent of alterations in G protein-coupled receptors and/or G proteins (Bavencoffe et al.,
87 2016). Analgesic effects of opioids and cannabinoids depend upon the coupling of these
88 modulators' receptors to Gαi family members. Thus, an SCI-induced decrease in AC sensitivity
89 to Gαi proteins indicates a reduction in the sensitivity of cAMP production in nociceptors to both
90 endogenous and clinically applied opioids that might exacerbate chronic pain (Sun et al., 2019).
91 How this insensitivity to opioid signaling is produced and how it integrates with the other
92 alterations observed in nociceptor function after SCI are not known.

93 Our observations that SCI induces chronic depolarization of nociceptors (Bavencoffe et
94 al., 2016; Odem et al., 2018; Berkey et al., 2020) and decreases Gαi-mediated inhibition of

95 cAMP production led to the hypothesis that SCI-induced depolarization of resting membrane
96 potential (RMP) plays a major role in driving the reduced responsiveness to opioids. Combining
97 high content microscopy, cluster analysis and electrophysiology, we have tested this hypothesis
98 and defined a critical signaling pathway. We confirm that months after SCI in intact rats, DRG
99 neurons in culture are less sensitive to the mu opioid receptor (MOR) agonist DAMGO and we
100 show that this phenomenon is largely restricted to the subpopulation of DRG neurons that bind
101 isolectin B4 (IB4), a marker of non-peptidergic nociceptors. Importantly, reduced opioid
102 sensitivity is induced in nociceptors from naive rats by artificial depolarization of RMPs similar to
103 the depolarized RMPs found in spontaneously active nociceptors after SCI. The reduced opioid
104 sensitivity is produced at least in part by depolarization activating components of the ERK
105 pathway, including increased phosphorylation of C-Raf (S338) and phosphorylation-induced
106 inhibition of C-Raf inhibitor RKIP (S153). Disinhibition and activation of C-Raf by depolarization
107 shifts the dose-response curve of DAMGO to higher concentrations in DRG neurons from naive
108 and SCI rats. Moreover, in non-excitable HEK293 cells activation of C-Raf or expression of an
109 activated form of C-Raf also reduces the sensitivity of AC to the effects of opioids. The resulting
110 ERK activity downstream from C-Raf is not necessary for the reduced responsiveness to
111 opioids, but in sensory neurons ERK is required to maintain depolarized RMP and hyperactivity
112 after SCI, demonstrating a positive feedback relationship between depolarization and ERK
113 activity. Our results not only provide a novel mechanism linking opioid insensitivity to nociceptor
114 hyperexcitability in a chronic pain state, but also reveal an unexpected feedback function for the
115 persistent depolarization of RMP that is associated with SCI and many other chronic pain
116 conditions to recurrently stimulate cell signaling pathways important for maintaining the
117 nociceptor depolarization and other hyperexcitable alterations that persistently drive pain.

118

119 **Materials and Methods**

120 **Antibodies and Reagents**

121 Primary antibodies: Rabbit monoclonal anti-phospho RII (S99) (1:1000, clone 151, Abcam, #
122 ab32390), mouse monoclonal anti phospho-p44/42 MAPK (T202/Y204) (1:300, clone E10, Cell
123 Signaling, # 9106), anti-phospho RKIP (S153) (1:500, polyclonal, Santacruz # sc-32622), anti-
124 phospho C-Raf (S338) (1:500, Cell signaling, # 9427), anti-CGRP (1:1000, Santacruz # SC-
125 57053), anti-PGP9.5 (1:4000, Novus Biologicals, # NB110-58872). Secondary antibodies (all
126 1:1000): Goat anti-chicken- DyLight 755, Goat anti-mouse Alexa Fluor (AF) 750, donkey anti-
127 mouse AF 647, 568, 488, Goat anti-rabbit AF 568, 488 were purchased from ThermoFisher.
128 Isolectin B4-FITC (1:1500, MilliporeSigma, # L2895) DAPI.

129 Drugs: retigabine and inhibitors for C-Raf (GW5074), pan-Raf (RAF709), ERK (UO126), PKA
130 (H89), PKC (sotrastaurin), and Src (saracatinib) were purchased from Selleck Chemicals
131 (Houston, TX). Forskolin and morphine sulfate were purchased from Cayman Chemicals (Ann
132 Arbor, MI). DAMGO was purchased from Bachem (Switzerland). All drugs were prepared as
133 stock solutions in PBS (morphine, DAMGO), or DMSO (retigabine, GW5074, RAF709, UO126,
134 H89, Sotrastaurin, Saracatinib, forskolin) and kept as aliquots at -20°C. Raf-CTH was a gift from
135 Dr. John Hancock (UTHealth) and represents a fusion of Raf-1 (C-Raf) with the complete
136 carboxy-terminal hypervariable region of H-Ras, resulting in plasma membrane targeting and
137 Raf activation (Inder et al., 2008).

138 **Animals**

139 All procedures followed the guidelines of the International Association for the Study of Pain and
140 were approved by the McGovern Medical School at UT Health Animal Care and Use
141 Committees. Male Sprague-Dawley rats (Envigo, USA) (8-9 weeks old, 250-300g, 2 per cage)
142 were allowed to acclimate to a 12-hour reverse light/dark cycle for at least four days before

143 beginning experiments. Sex differences between male and female rats in nociceptor
144 hyperactivity have been noted after SCI (Bedi et al., 2010) and, like other pain-related
145 phenomena (Mogil, 2020), these may involve complex sex-specific mechanisms. Possible sex
146 differences in the mechanisms addressed in this report are under separate investigation by the
147 authors.

148 **Spinal cord injury (SCI) procedures**

149 Surgeries were conducted as previously described (Bedi et al., 2010; Wu, 2013; Yang et al.,
150 2014; Bavencoffe et al., 2016; Berkey et al., 2020). Rats were anesthetized with isoflurane
151 (induction 4-5%; maintenance 1-2%, Henry Schein, Dublin, OH). A T10 vertebral laminectomy
152 was followed by a dorsal contusive spinal impact (150 kilodyne, 1-second dwell time) using an
153 Infinite Horizon Spinal Cord Impactor (Precision Systems and Instrumentation, LLC, Fairfax
154 Station, VA). Sham-operated rats received the same surgical treatment without the contusion.
155 The analgesic buprenorphine hydrochloride (0.02 mg/kg in 0.9% saline 2 ml/kg; Buprenex,
156 Reckitt Benckiser Healthcare Ltd., Hull, England, UK) and the antibiotic enrofloxacin (0.3 ml in
157 0.9% saline; Enroflox, Norbrook, Inc., Overland Park, KS) were injected i.p. twice daily for 5
158 days (buprenorphine) or 10 days (enrofloxacin). Manual bladder evacuations were performed
159 twice daily until rats recovered neurogenic bladder voiding. Rats had free access to food and
160 water. All rats included in this study received a score of 0 or 1 for both hind limbs the day after
161 surgery, as measured on the Basso, Beattie, and Bresnahan (BBB) Locomotor Rating Scale
162 (Basso et al., 1995). Tissue from SCI or Sham rats was harvested 1 to 3 months post-surgery.
163 In this study most of the controls were uninjured, naive rats. In our initial experiments, sham-
164 operated rats were also examined and found to show no apparent differences in biochemical
165 responses to opioids compared to sham-operated rats, similar to previous observations of
166 relatively little difference in electrophysiological properties between naïve and sham-surgery
167 control groups (Bedi et al., 2010; Bavencoffe et al., 2016; Odem et al., 2018). Naïve and sham-

168 surgery controls were therefore pooled into a single Control (Ctrl) group for these experiments
169 (Fig.1), whereas in the subsequent experiments only a Naïve (Nv) control group was used.

170 **DRG neuron cultures**

171 DRGs were harvested below vertebral level T10. Ganglia were surgically desheathed before
172 being transferred in high-glucose DMEM culture medium (Sigma-Aldrich, St Louis, MO)
173 containing trypsin TRL (0.3 mg/ml, Worthington Biochemical Corporation, Lakewood, NJ) and
174 collagenase D (1.4 mg/ml, Roche Life Science, Penzberg, Germany). After 40 minutes
175 incubation under constant shaking at 34°C, digested DRG fragments were washed by two
176 successive centrifugations and triturated with a fire-polished glass Pasteur pipette. For imaging
177 experiments, cells were further subjected to BSA gradient centrifugation (BSA, 15%) to remove
178 disrupted cell debris. For high-content imaging, cells were plated on 96 well plates (Greiner Bio-
179 One, Germany) coated with poly-L-ornithine at a density of ~300-500 neurons per well and
180 incubated overnight DMEM 37°C, 5% CO2 and 95% humidity in absence of growth factors or
181 supplements. For electrophysiology, cells were plated on 8 mm glass coverslips coated with
182 poly-L-ornithine (Sigma-Aldrich, St Louis, MO) in DMEM without serum or growth factors, and
183 incubated overnight at 37°C, 5% CO2 and 95% humidity.

184 **HEK-293 cultures and transfection**

185 HEK-293 cells stably expressing the mu opioid receptor were maintained at 37°C with 5% CO2
186 in Dulbecco's modified Eagle's medium supplemented with 10% fetal bovine serum and 100
187 µg/ml Hygromycin B. Cells were seeded at 2.5×10^5 cells per well in a 6 well plate and
188 transfected the next day with RAF-CTH or pCDNA3 (10 µg total DNA per well) using
189 Lipofectamine 2000 (Invitrogen). Medium was replaced 4 hr after transfection. Cells were re-
190 plated 24 hours after transfection into 96 well plates at $1x10^4$ cells per well. Unless indicated,

191 cells where serum starved 4 hours prior stimulation. Drug treatments, fixation and staining were
192 performed 48 hours post-transfection as described for neuronal cultures.

193 **Cell treatments and immunofluorescence staining**

194 Neuronal cultures were treated with the indicated reagents 24 h after plating. All experiments
195 and incubations were performed at 37°C. Pharmacological treatments were performed using a
196 modified protocol detailed in (Isensee et al., 2014). Neurons were pretreated with inhibitors for
197 30 min prior to simultaneous addition of forskolin, extracellular potassium, and/or DAMGO for 5
198 min. Compounds were added by removing half of the supernatant in the culture well, mixing it
199 with 10x compound in 96-well-V-bottom plates using automatic multichannel pipettes, prior to
200 addition back to the same culture well to reach final concentrations of compound. Controls were
201 treated similarly, mixing the supernatant with vehicle (PBS ± DMSO). For compounds dissolved
202 in DMSO, the final DMSO concentration in culture medium was ≤ 0.1%. Cells were fixed with
203 4% paraformaldehyde (10 min at 22°C) and washed twice with PBS. Blocking and
204 permeabilization of fixed cells were performed in a single step using blocking buffer (1% BSA,
205 0.075% Triton X-100, 1 hr, RT). Subsequently, the cultures were incubated with primary
206 antibodies diluted in blocking buffer at 4°C overnight, washed, and incubated with DAPI (1:100)
207 and secondary Alexa dye-coupled antibodies in blocking buffer (1:1000, 1h, RT). In the case of
208 IB4 staining (1:1500), incubations were conducted simultaneously or after the secondary
209 antibody staining in IB4 buffer (PBS + 0.1 mM Ca^{2+}, 0.1 mM Mg^{2+}, 0.1 mM Mn^{2+}, 1h RT)
210 followed by three final PBS washes (10 min, RT). After the final wash the plates were sealed
211 and immediately imaged or stored at 4°C until imaging.

212 **Quantitative high-content microscopy**

213 We used a modification of the protocols implemented by (Isensee et al., 2014; Isensee et al.,
214 2017; Isensee et al., 2018). Stained cultures in 96-well plates were scanned using a Cellomics

215 CX5 microscope (Thermo scientific). Images of 1104x1104 pixels were acquired with a 10x
216 objective and analyzed using the Cellomics software package (Thermo scientific). After
217 background correction, neurons were identified based on PGP 9.5 staining intensity. Object
218 segmentation was performed using the geometric method. When required, spillover between
219 channels was compensated in the post-analysis using raw fluorescence data from fluorescence
220 controls (PGP 9.5 alone; PGP 9.5 + antibody 1; and PGP 9.5 + antibody 2). The slope of best
221 linear fit was determined by linear regression (Prism, GraphPad) and used to compensate spill-
222 over as described (Roederer, 2002). Results for each condition consist of at least 3 different
223 replicate experiments performed on different days.

224 **Electrophysiology**

225 Whole-cell patch clamp recordings were performed at ~ 21°C 18-30 hours after dissociation
226 using an EPC10 USB (HEKA Elektronik, Lambrecht/Pfalz, Germany) amplifier. Patch pipettes
227 were made of borosilicate glass capillaries (Sutter Instrument Co., Novato, CA) with a horizontal
228 P-97 puller (Sutter Instrument Co., Novato, CA) and fire-polished with a MF-830 microforge
229 (Narishige, Tokyo, Japan) to a final pipette resistance of 3-8 MΩ when filled with an intracellular
230 solution composed as follows (in mM): 134 KCl, 1.6 $MgCl_2$, 13.2 NaCl, 3 EGTA, 9 HEPES, 4
231 Mg-ATP, and 0.3 Na-GTP, adjusted to pH 7.2 with KOH and 300 mOsM with sucrose. Isolated
232 neurons with a soma diameter ≤ 30 μM were observed at 20x magnification on IX-71 (Olympus,
233 Tokyo, Japan) inverted microscope and recorded in a bath solution containing (in mM): 140
234 NaCl, 3 KCl, 1.8 $CaCl_2$, 2 $MgCl_2$, 10 HEPES, and 10 glucose, which was adjusted to pH 7.4 with
235 NaOH and 320 mOsM with sucrose. After obtaining a tight seal (>3 GΩ), the plasma membrane
236 was ruptured to achieve whole-cell configuration under voltage clamp at -60 mV. All subsequent
237 recording was under current clamp using Patchmaster v2x90.1 (HEKA Elektronik, Lambrecht /
238 Pfalz, Germany). Depolarizing spontaneous fluctuations of membrane potential (DSFs) were
239 measured with a custom automated program (SFA_pub.py). Procedures for measurements of

240 DSFs (minimum cutoffs, 1.5 mV amplitude, 10 ms duration), spontaneous activity (SA) at resting
241 membrane potential (RMP), ongoing activity at a holding potential of -45 mV (OA), action
242 potential (AP) voltage threshold, and rheobase at a holding potential of -60 mV are described by
243 Odem et al. (2018). To permit direct comparison with our previous publications and many
244 others, the liquid junction potential (calculated to be ~4.3 mV using pClamp software and the
245 algorithm developed by (Barry, 1994)) was not corrected. This means that actual membrane
246 potentials were ~4 mV more negative than the values reported in this article.

247 **Data analysis**

248 One- and two-dimensional probability density plots were generated using FlowJo (Becton
249 Dickinson, Ashland, OR). Gating of subpopulations was performed by setting thresholds at local
250 minima of probability density plots. Individual cells used to perform the cluster analysis were
251 normalized between the minimal (0.001%) and maximal (0.999%) fluorescence levels per
252 channel, per experiment. Cluster analysis (k-medians) was performed using software Cluster
253 3.0 (de Hoon et al., 2004). Three-dimensional (3D) plots were constructed using Plotly (Chart
254 Studio, Waltham, MA). Data analysis and graph plots were performed using Prism (v7.03 and
255 V8.0) (GraphPad Software, Inc, La Jolla, CA).

256 **Statistics**

257 **HCM:** Data averaged across all neurons of a given type from a single animal represent a single
258 data point (n=1). For cultured cell lines, every plate from independent cultures is considered
259 n=1. Repetition of the same treatment within an experiment from a single animal or plate
260 provides internal replicates and the average is reported with n=1. At least 3 independent
261 experiments from different animals, performed on separate dates (n=3) are reported for every
262 data set. HCM data are presented as mean ± SEM or box-whisker plots indicating the full data
263 range, quartiles, median and mean. All data sets were tested for normality with the Shapiro-Wilk

264 test. Outliers to be excluded form analysis were identified using the ESD method ($p<0.05$).
265 Normally distributed data were tested with parametric tests: *t*-test, 1-way or 2-way ANOVA
266 followed by Tukey's test, Dunnett's multiple comparisons test or Sidak's multiple comparisons
267 test for each pair-wise comparison. Statistical significance was set at $P < 0.05$ (*) and all
268 reported values are two-tailed. In the case of non-normally distributed data (Figure 1D), data
269 were compared using the Mann Whitney test. Statistical analysis and fits of dose-response
270 curves were performed using Prism v8.01 (GraphPad Software, Inc, La Jolla, CA).

271 Electrophysiology: All data are presented as mean ± SEM, except where noted for
272 electrophysiological measurements of OA (presented as incidence (%) of neurons sampled). All
273 data sets were tested for normality with the Shapiro-Wilk test. Normally distributed data were
274 tested with parametric tests 1-way ANOVA or Brown-Forsythe and Welch ANOVA tests followed
275 respectively by Holm-Sidak's or Dunnett's multiple comparisons tests for each pair-wise
276 comparison using Prism v8 (GraphPad Software, Inc, La Jolla, CA). Non-normally distributed
277 sets of data were tested with Kruskal-Wallis test followed by Dunn's multiple comparison test.
278 Comparisons of incidence were made using Fisher's exact test with Bonferroni corrections for
279 multiple comparisons. Statistical significance was set at $p< 0.05$ (*) and all reported values are
280 two-tailed. Details of all statistical analysis can be found in Table 1.

281 **Results**

282 **SCI reduces the opioid sensitivity of IB4$^+$ nociceptors.** Previous biochemical data show a
283 decreased sensitivity to Gαi-mediated inhibition of AC activity in DRG membranes after SCI
284 (Bavencoffe et al., 2016). The reduced sensitivity was receptor-independent, as AC activity was
285 tested with exogenously added purified GTPγS-activated G proteins. To test if this extends to
286 regulation by opioids of the intact cell bodies of DRG neurons, DRG neurons were cultured
287 overnight after isolation from SCI and control rats 1 to 3 months after injury. Production of cAMP
288 was induced by forskolin (Fsk 3 μM, 5 min), while opioid responses were simultaneously
289 stimulated by the highly selective mu opioid receptor (MOR) agonist DAMGO. Using
290 phosphorylation of the RII regulatory subunit of PKA (PKA-pRII, Fig. 1A) as a surrogate
291 measure of cAMP responses (detailed in (Isensee et al., 2018)), DAMGO effects were
292 calculated as the inhibition of forskolin-induced phosphorylation of PKA-RII. Extending our
293 previous observations on isolated DRG membranes using activated Gαi proteins (Bavencoffe et
294 al., 2016), DAMGO effects on cAMP production were reduced in cultured neurons from SCI rats
295 (Fig. 1B, $p<0.05$), yielding a 3-6 fold increase in the IC_{50} for DAMGO in the SCI group compared
296 to the pooled (naïve and sham-operated) Control (Ctrl) group (Fig. 1C, D: IC_{50}, Ctrl =
297 0.053±0.0063, SCI = 0.21±0.047, Mann Whitney test, $p=2x10^{-5}$). No significant differences were
298 found between the Naïve and Sham groups (not shown).

299 Because DRG neurons constitute a highly heterogeneous population with discrete
300 neuronal types associated with specific markers and functional specializations, we proceeded to
301 analyze SCI vs. Naive responses to DAMGO in distinct neuronal subgroups in culture. To this
302 end, we used a combination of high content microscopy data and K-means cluster analysis to
303 separate DRG neurons into different subpopulations based on size (cell body area), CGRP
304 expression (characteristic of peptidergic nociceptors) and isolectin B4 binding (IB4, a marker of
305 non-peptidergic nociceptors). These three parameters were combined in a 3D space plot where

306 every neuron was represented by coordinates for its area, CGRP expression, and degree of IB4
307 binding (Fig. 2A). The phosphorylation of PKA-pRII was then mapped onto these 3D
308 coordinates to reveal differences in cAMP signaling for each cluster (Fig. 2B). DRG neurons
309 cultured from both naive and SCI rats could be differentiated into 7 distinct clusters (Fig. 2A, C),
310 with no significant differences in cluster sizes between SCI and Naive groups (Fig. 2D). As
311 expected, cAMP/PKA-pRII responses to forskolin were observed in all 7 neuronal clusters, with
312 particular prominence in the $IB4^+/CGRP^-$ subgroups (Fig. 2E). Significant DAMGO inhibition of
313 forskolin responses was present in medium-sized and small neurons in $IB4^+$ and $CGRP^+$
314 neurons from naive animals, confirming previous reports of MOR mRNA expression in both
315 small $IB4^+$ and $IB4^-$ DRG neurons (Wang et al., 2010). While no significant differences in
316 maximal forskolin responses were observed between SCI and Naive groups, DAMGO effects
317 were specifically impaired in $IB4^+/CGRP^-$ neurons (IB4) from SCI animals (Fig. 2E), with a ~50%
318 reduction in the overall DAMGO effect compared to $IB4^+$ neurons from naive animals (54%
319 versus 27% inhibition, p=0.014, unpaired t test). Within the $IB4^+/CGRP^+$ group (IB-CG), we also
320 observed a trend towards reduced DAMGO responses after SCI (p=0.053, unpaired t test).

321 **Acute depolarization reduces the opioid sensitivity of $IB4^+$ nociceptors.** We have
322 previously shown that capsaicin-sensitive and $IB4^+$ DRG neurons (probable nociceptors)
323 dissociated from SCI animals show multiple hyperexcitable alterations, including depolarized
324 RMP, reduced thresholds for generating action potentials, and an increased occurrence of
325 spontaneous activity (SA) – which normally is quite rare in primary nociceptors (Bedi et al.,
326 2010; Odem et al., 2018). Electrical activity in nociceptors can be promoted by the activation of
327 multiple downstream signaling cascades (Salzer et al., 2019). An interesting general question is
328 whether some of these cascades can also be activated recurrently by the ongoing
329 depolarization of RMP that usually occurs in hyperactive nociceptors (Bavencoffe et al., 2016;
330 Odem et al., 2017; Berkey et al., 2020). Specifically, we asked whether 5-min depolarization of

331 RMP in nociceptors isolated from naive rats, produced by increasing extracellular K^+
332 concentration ($[K^+]_e$), is sufficient to decrease neuronal sensitivity to DAMGO. RMP measured at
333 several $[K^+]_e$ (Fig. 3A) was associated with changes in ERK and PKA responses in the general
334 DRG neuronal population (Fig. 3B, C). Interestingly, neurons in the SCI group exhibited a
335 significantly more depolarized RMP compared to the Naive group at normal (3 mM) and
336 modestly elevated (10 mM) extracellular K^+ concentrations (Fig. 3A), but the RMPs converged
337 at higher $[K^+]_e$. In agreement with previous findings in PC12 cells and primary cortical neurons
338 (Rosen et al., 1994), increasing $[K^+]_e$ activated ERK by phosphorylation in both Naive and SCI
339 groups. Significant ERK activation was found at RMPs at or more depolarized than -45 mV (15
340 mM $[K^+]_e$), suggesting a threshold for ERK activation near -45 mV in the Naive and SCI groups,
341 with an additional enhancement of ERK activation by SCI above this threshold (Fig. 3B;
342 p=0.0022, 2-way ANOVA). The depolarization-enhanced phosphorylation of ERK occurred at
343 much lower $[K^+]_e$ (13 to 15 mM, resulting in RMPs of approximately -50 to -40 mV) than those
344 used in studies of other cell types (e.g. 50-100 mM $[K^+]_e$, producing RMPs of -10 to 0 mV
345 (Rosen et al., 1994; Baldassa et al., 2003)). PKA was also activated by depolarization, but
346 without any difference between Naive and SCI groups (Fig. 3C). Depolarization from RMP
347 (usually between -65 and -55 mV) to -45 mV is modest relative to normal action potential (AP)
348 threshold (~-35 mV) in nociceptors from naïve rats, and it rarely evokes action potentials in
349 these neurons (Odem et al., 2018). Importantly, after SCI, -45 mV is a sufficiently depolarized
350 RMP for large depolarizing spontaneous fluctuations (DSFs) to reach the reduced AP threshold
351 and generate spontaneous activity (SA) (Odem et al., 2018). Using IB4 binding to distinguish
352 between neuronal subgroups, our results show that the increased ERK activation by modest
353 depolarization after SCI is specific to $IB4^+$ neurons (p=0.047, 2-way ANOVA), with no significant
354 difference between Naive and SCI groups for $IB4^-$ neurons (Fig. 3D).

355 **Depolarization-induced reduction of opioid sensitivity requires signaling by C-Raf.** To
356 demonstrate the predicted link between depolarized RMP in nociceptors produced by SCI and
357 reductions in opioid sensitivity and associated ERK signaling, we tested the influence of RMP
358 on opioid sensitivity. Neurons from the uninjured Naive group were exposed to 15 mM $[K^+]_e$
359 alone or concurrently with the 5-min Fsk or Fsk + DAMGO stimulation (Fig. 3E). RMP
360 depolarized from approximately -65 mV to about -45 mV during the stimulation (Fig. 3A) –
361 reaching the optimal range of RMP for generation of large DSFs and sustained ongoing activity
362 after SCI (Odem et al., 2018). This modest depolarization gave rise to a small, ~20%, increase
363 in basal cAMP/PKA-pRII responses, consistent with the low expression of AC1/8 in DRGs
364 (Bavencoffe et al., 2016; Dessauer et al., 2017). Overall forskolin responses were unchanged
365 by SCI (Fig. 1B) or by 15 mM $[K^+]_e$ in the Naive group. Under these conditions, depolarization
366 had a striking effect on DAMGO sensitivity, dramatically decreasing DAMGO inhibition of
367 forskolin responses compared to 5 mM $[K^+]_e$ control (Fig. 3E, p=0.0015, 2-way ANOVA);
368 resulting in a 1.5-fold increased IC_{50} and ~50% decreased efficacy (E_{max}) for DAMGO compared
369 to 5 mM $[K^+]_e$ control (Fig. 3F; $p=4x10^{-29}$, 2-way ANOVA; quantitated further in Fig 4C, D).
370 Depolarization also decreased overall inhibition of forskolin responses by morphine, a non-
371 peptidic MOR agonist, compared to control (Fig 3G; p=0.0009, 2-way ANOVA), resulting in a 7-
372 fold increase in the IC_{50} (Fig. 3G). The reduced DAMGO efficacy is likely at the level of MOR, as
373 the reduction in E_{max} is not observed with the partial agonist morphine (Fig. 3F, G), and is similar
374 to the voltage-dependent reduction in efficacy observed with other GPCRs (Vickery et al.,
375 2016). Moreover, regulation of MOR by voltage was recently reported (Ruland et al., 2020).

376 The rapid onset of $[K^+]_e$-induced effects (within 5 min) indicates that under these testing
377 conditions the observed effects are independent of transcription and/or translation, and point
378 towards direct signaling events triggered by depolarization. To determine which signaling
379 pathways are required for the depolarization-induced shift in DAMGO responses, DRG neurons

380 were pretreated with inhibitors of Src, PKC, PKA, Raf and MEK for 30 min to test for their ability
381 to block reductions in DAMGO responses by 15 mM $[K^+]_e$. Selective C-Raf (GW5074) and pan-
382 Raf (RAF709) inhibitors blocked the effects of 5-minute depolarization when tested with 0.1 μM
383 DAMGO (Fig. 4A, p=0.0082, 1-way ANOVA). Interestingly, the C-Raf inhibition (3 μM, 30 min)
384 appeared to reverse the increase in DAMGO IC_{50} induced by 15 mM $[K^+]_e$ (Fig, 4B, C: Ctrl vs
385 K^+15(-): p=0.013; K^+15(-) vs K^+15(GW): p=0.034, 1-way ANOVA), but not the alteration in
386 DAMGO E_{max} (Fig. 4B, D: Ctrl vs K^+15(-): p=3x10^{-8}, 1-way ANOVA). In contrast, under control
387 conditions (5 mM $[K^+]_e$), GW5074 pretreatment had no effects on DAMGO sensitivity (Fig 4B,
388 dotted line). The lack of effects by inhibitors of MEK or PKC (UO126 and sotrastaurin,
389 respectively), suggest that signaling previously reported to modulate MOR responses via
390 receptor desensitization (ERK, (Polakiewicz et al., 1998)) or phosphorylation of Gαi2 (PKC,
391 (Strassheim and Malbon, 1994)) are not required for depolarization-induced reductions in
392 DAMGO sensitivity.

393 Raf activation is complex and involves several mechanisms, including but not limited to
394 Ras-mediated recruitment of Raf to the cell membrane followed by multiple phosphorylations via
395 different protein kinases that enhance C-Raf catalytic activity (S338 among the best studied;
396 reviewed in (Leicht et al., 2007)). In addition, C-Raf signaling requires relief of inhibition by RKIP
397 via the phosphorylation of RKIP-S153 (Fig. 5A; (Corbit et al., 2003)). To examine which of these
398 mechanisms are triggered by depolarization of nociceptors, we examined the effect of $[K^+]_e$–
399 induced depolarization (5 min) on RKIP-S153 and C-Raf-S338 phosphorylation in the total DRG
400 neuronal population (Fig. 5B). Depolarization triggered a rapid, dose-dependent increase in C-
401 Raf and RKIP phosphorylation, rising steeply as a function of $[K^+]_e$ with an EC_{50} of 14.72 ± 0.40
402 mM for pC-Raf and 13.11± 0.41 mM for pRKIP (corresponding to a RMP of approximately -46
403 mV and -48 mV for pC-Raf and pRKIP, respectively). As observed for pERK, $[K^+]_e$ 15 mM
404 induced significantly higher phosphorylation of C-Raf in the SCI group (Fig 5C, p=0.038,

405 unpaired *t* test). Depolarization-induced phosphorylation of C-Raf and RKIP occurred in several
406 types of DRG neurons, with the highest increases detected in the small soma size, IB4$^+$ group
407 (Fig. 5D and E, Fig 5F lower left quadrant of the 3D cluster maps; Fig. 5G). C-Raf directly
408 phosphorylates and regulates Gαi-sensitive AC isoforms (Tan et al., 2001; Ding et al., 2004).
409 Therefore, to demonstrate that C-Raf activation is sufficient to decrease DAMGO sensitivity, we
410 expressed a membrane-targeted active C-Raf construct in HEK293 cells stably expressing the
411 MOR (Fig. 6). Transient expression of plasma membrane targeted C-Raf gave rise to a 2.2-fold
412 shift in the IC_{50} for DAMGO (Fig. 6B, p=0.0028, 1-way ANOVA) with no alterations in the E_{max}
413 (Fig. 6A, C). Serum treatment had similar effects, producing a 2.8-fold shift in the DAMGO IC_{50}
414 (p=0.016, 1-way ANOVA) that was reversed by the C-Raf inhibitor GW5074 (p=0.026, 1-way
415 ANOVA). Interestingly, while treatment of non-excitable HEK293 cells with 15 and 50 mM $[K^+]_e$
416 did not alter the IC_{50} of DAMGO or induce activation of C-Raf (Fig. 6B and data not shown),
417 $[K^+]_e$ dose-dependently reduced the E_{max} of DAMGO (10% and 47% reduction in E_{max},
418 respectively; p=4x10^{-4} and p< 0.0001, 1-way ANOVA) (Fig. 6C). Thus treatment with $[K^+]_e$
419 requires C-Raf activation to alter DAMGO potency, while the effects of depolarization on
420 DAMGO E_{max} may indeed indicate a voltage-sensitive mechanism acting directly on the mu-
421 opioid receptor (Vickery et al., 2016; Ruland et al., 2020).

422

423 **Reduction of opioid sensitivity and production of hyperexcitability by SCI are reversed**
424 **by treatments that inhibit C-Raf signaling or hyperpolarize RMP.** We next tested whether
425 inhibition of C-Raf or reversing the SCI-mediated depolarization of nociceptors is sufficient to
426 restore DAMGO responses after SCI. Inhibition of C-Raf with the selective C-Raf inhibitor,
427 GW5074 restored the IC_{50} of DAMGO in nociceptors from SCI rats to that found in the Naive
428 group (Fig. 7A). A clinically relevant approach to reversing depolarization is to open K^+ channels
429 pharmacologically. KCNQ (M-type) channels contribute ~9 mV to the RMP of capsaicin-

430 sensitive nociceptors, and application of the KCNQ channel opener, retigabine (10 μM) is
431 reported to produce an additional 10 mV hyperpolarization of RMP (Du et al., 2014). Moreover,
432 10 μM retigabine was shown to hyperpolarize small DRG neurons isolated from SCI rats (Wu et
433 al., 2017). We found that this dose of retigabine restored the IC_{50} of DAMGO for the SCI group
434 to a value close to that of the Naive group (Fig. 7A, B and 1D; IC_{50}, Naive = 0.053±0.006 and
435 retigabine = 0.023±0.009). Hyperexcitability of nociceptors induced by SCI is manifested not
436 only as depolarized RMP, but also as spontaneous activity (SA) at RMP in vivo and in vitro
437 (Bedi et al., 2010) and enhanced ongoing activity (OA) revealed during prolonged experimental
438 depolarization to -45 mV (Odem et al., 2018). Pre-treatment of neurons from SCI rats with
439 inhibitors of C-Raf (GW5074) or MEK (UO126) blocked SA and OA and led to a
440 hyperpolarization of RMP (Fig. 7C-E; Control = -53 ± 2 mV, GW5074= -62 ± 2 mV, UO126 = -62
441 ± 3 mV), whereas pre-treatment of DRG neurons from naive rats with UO126 had no effect on
442 SA, OA, or RMP (data not shown; RMP Control = -66 ± 2 mV, n=14; UO126 = -65 ± 2 mV, n=9;
443 GW5074 = -60 ± 3 mV, n=8; Kruskal-Wallis with Dunn's multiple comparison, p=0.14). Inhibition
444 of C-Raf and MEK also reduced another functional contribution to SCI-induced hyperactivity in
445 nociceptors - the enhancement of depolarizing spontaneous fluctuations of membrane potential
446 (DSFs) that bridge the gap between RMP and AP voltage threshold to trigger APs (Odem et al.,
447 2017). The mean amplitude of DSFs (subthreshold and suprathreshold) was significantly
448 reduced when treated with GW5074 or UO126 and assayed at a holding potential of -45 mV
449 (Fig. 7F), as was the amplitude of the subthreshold DSFs alone (p=0.015 for GW5074, p=0.013
450 for UO126, Kruskal-Wallis with Dunn's multiple comparison, data not shown). DSF amplitudes
451 were not significantly reduced when measured at RMP, at least in part because DSFs are
452 voltage-dependent (Odem et al., 2018) and RMPs are quite variable (Fig. 7E). When tested on
453 nociceptors from SCI, only UO126 increased the rheobase (data not shown in figure: vehicle =
454 35 ± 7 pA; GW5074 = 57 ± 16 pA, n.s.; UO126 = 83 ± 14 pA, p=0.006, Kruskal-Wallis with
455 Dunn's multiple comparison), while neither drug had a significant effect on AP threshold (data

456 not shown, Brown-Forsythe and Welsh Tests). C-Raf/ERK and cAMP pathways are thus both
457 required to maintain the increased excitability after SCI (Fig. 7D-F; Bavencoffe et al 2016;
458 Berkey et al 2019). C-Raf activation of its canonical downstream target, MEK, produces an
459 ERK-dependent positive feedback loop that helps to maintain increased spontaneous activity
460 and depolarized RMP chronically after SCI. In addition, C-Raf effects on AC (independent of
461 MEK-ERK activation) promote cAMP signaling by decreasing its inhibition from opioid/Gαi
462 signaling (Fig. 8). Note that when depolarization is produced by elevating extracellular K^+ (i.e.
463 without the need for any cell signaling input), inhibition of ERK has no direct effect on opioid
464 responsiveness. This finding suggests that the activation of C-Raf by SCI-induced
465 depolarization of RMP (and perhaps other manifestations of hyperexcitability) triggers two
466 independent signaling pathways acting in parallel to maintain the nociceptor hyperexcitable
467 state (Fig. 8).

468 **Discussion**

469 Previously, we showed that SCI causes a profound reduction of Gαi-mediated inhibition of AC
470 activity independent of endogenous receptors or G proteins, as revealed by comparing purified
471 G protein-stimulated DRG membranes from naive and SCI rats (Bavencoffe et al., 2016). The
472 present study shows that in vitro SCI-induced reduction of Gαi inhibition I) also occurs in intact
473 cell bodies of DRG neurons in dissociated cell culture, II) is most prominent in IB4$^+$ nociceptors,
474 III) is produced unexpectedly by modest depolarization of RMP, and IV) requires signaling
475 through C-Raf. Moreover, while ERK activity is not required for effects on opioid insensitivity,
476 ERK is necessary for SCI-induced nociceptor hyperexcitability. These findings provide new
477 insight into the signaling within primary nociceptors that reduces sensitivity to endogenous and
478 therapeutic opioids, and that may promote ongoing pain through multiple mechanisms, including
479 a previously unappreciated signaling role for RMP.

480 **Depolarization-induced effects on MAPK and cAMP signaling.** Depolarization of RMP
481 (typically produced experimentally by elevating $[K^+]_e$) has long been known to stimulate cellular
482 signaling, including signaling by mitogen-activated protein kinase (MAPK) cascades (Rosen et
483 al., 1994). Depolarization-induced signaling is often assumed to be mediated by increases in
484 cytoplasmic Ca^{2+} due to activation of voltage-gated Ca^{2+} channels, although other voltage-
485 sensitive, Ca^{2+}-independent mechanisms can contribute to ERK activity (reviewed in
486 (McLaughlin and Levin, 2018)). In rat DRG neurons, depolarization by 15 mM $[K^+]_e$ induced a
487 rapid and robust activation of ERK and phosphorylation of its upstream regulators, RKIP and C-
488 Raf. Observed predominantly in IB4$^+$ neurons, these responses occurred at physiological RMPs
489 that normally are subthreshold for evoking action potentials (-50 to -40 mV). The ERK
490 responses to depolarization were further enhanced by SCI. Importantly, -45 mV is within the
491 RMP range where, after SCI, large DSFs can reach AP threshold to generate sustained
492 spontaneous and ongoing activity (Odem et al., 2018; Berkey et al., 2020). Note that the actual

493 MP should be approximately 4 mV more negative than the values presented because our
494 measurements were not corrected for the liquid junction potential (see Methods).

495 Depolarization of RMP also induced a ~20% increase in basal cAMP/PKA signaling,
496 similar to increases in cortical neurons that generate substantial cross-talk with the MAPK
497 pathway (Baldassa et al., 2003). However, neither depolarization nor SCI altered forskolin-
498 stimulated AC activity in DRG neurons. Forksolin induced a robust cAMP response that was
499 inhibited by the mu-opioid receptor agonist DAMGO in $CGRP^+$ and $IB4^+$ DRG neurons from
500 naïve rats. Modest depolarization of naïve DRG neurons significantly blunted DAMGO inhibition
501 of cAMP responses in terms of both the IC_{50} and efficacy (E_{max}) of DAMGO, by independent
502 mechanisms. Reduction of DAMGO IC_{50} by depolarization was similar to that by SCI, both
503 requiring C-Raf activity. In contrast, depolarization effects on opioid efficacy were C-Raf
504 independent, agonist specific (morphine vs. DAMGO), and were observed in neurons and HEK
505 cells, suggesting a receptor-mediated mechanism. Voltage can modulate the efficacy of MOR
506 coupling to G proteins and β-arrestin in an agonist-specific manner (Ruland et al., 2020). Altered
507 balance of voltage-regulated G-protein/β-arrestin activation may explain our E_{max} effects at high
508 DAMGO concentrations.

509 **Molecular model for depolarization-dependent regulation of AC activity and ERK activity**
510 **that drives nociceptor hyperexcitability and opioid insensitivity after SCI.** The findings
511 discussed above suggest a model (Fig. 8) in which persistent depolarization of RMP after SCI
512 continuously activates the Ras/C-Raf/MEK/ERK cascade, at least in part via enhanced C-Raf
513 phosphorylation and relief of C-Raf inhibition by RKIP. While maintenance of hyperexcitability
514 requires concurrent ERK activation and cAMP signaling in nociceptors after SCI, activation of C-
515 Raf is sufficient to reduce AC inhibition by opioids independent of either ERK or PKA activity.
516 Based on our biochemical evidence from DRG membranes (Bavencoffe et al., 2016), this model
517 assumes that chronic reduction in Gαi-mediated inhibition of AC induced by SCI is due to a

518 modification of AC or a closely associated protein that regulates AC. C-Raf directly
519 phosphorylates AC5/6, but not AC1, on multiple serine residues (Ding et al., 2004) and co-
520 immunoprecipitates with AC6 (Ding et al., 2004; Beazely et al., 2005). Moreover, C-Raf
521 phosphorylation of AC6 in HEK293 cells leads to a 50% and 2-fold increase in basal and
522 forskolin-stimulated AC6 activity, respectively. However, regulation by Gαi was never tested. We
523 show that overexpression of activated C-Raf in HEK293 cells resulted in reduced DAMGO
524 sensitivity, but the effect was not as strong as that observed in DRG neurons. The MOR recruits
525 C-Raf via the scaffold Hint1 and facilitates phosphorylation of AC5/6 (Rodriguez-Munoz et al.,
526 2011; Zhang et al., 2013). Therefore, scaffolding and/or accessory proteins in DRG neurons
527 may facilitate C-Raf regulation of AC. Alternatively, AC isoforms expressed in DRGs versus
528 HEK293 cells may be more sensitive to C-Raf regulation. Importantly, none of our inhibitor or
529 overexpression studies supports a role for increased MOR desensitization or internalization
530 after SCI or depolarization in C-Raf-mediated effects. Depolarization increases delta OR
531 insertion into the membrane, but has no reported effect on MOR internalization (reviewed by
532 (Zhang et al., 2015)). Furthermore, peripheral MOR are upregulated, not downregulated, after
533 contusive thoracic SCI in mice (Liu et al., 2019).

534 Regulation of AC by C-Raf plays a key role in models of superactivation of AC
535 precipitated by removal of agonist after sustained treatment with morphine or agonists of other
536 Gi-coupled receptors. Inhibition of C-Raf attenuates superactivation of AC that occurs after long-
537 term opioid exposure (Varga et al., 2002). Additionally, inhibition or knockdown of C-Raf blunts
538 the development of thermal hyperalgesia, mechanical allodynia and antinociceptive tolerance
539 induced by sustained morphine treatment (Tumati et al., 2008). Although superactivation, like
540 SCI and depolarization, involves C-Raf, the similarities end there. Unlike superactivation, neither
541 depolarization nor SCI enhanced forskolin-stimulated cAMP production. Additionally,
542 depolarization-mediated reduction in DAMGO sensitivity occurred within 5 minutes, rather than

543 the 2-12 hours required for sustained morphine-induced superactivation (Varga et al., 2002).
544 Moreover, superactivation models depend on Src activation of C-Raf (Zhang et al., 2013),
545 whereas we found no effect of Src inhibition on depolarization-induced reductions of DAMGO
546 potency. These differences suggest that the mechanism by which superactivation versus SCI or
547 depolarization engage C-Raf for regulation of AC is distinct and context-dependent.

548 **Functional implications of depolarization-dependent C-Raf-ERK and C-Raf-AC signaling**
549 **in nociceptors.** In many experimental models of persistent pain, a continuing depolarization of
550 nociceptor RMP remains after excision of the ganglion or dissociation of the neurons. These
551 include nociceptors investigated not only in rodent SCI models (Odem et al., 2018; Berkey et al.,
552 2020), but also in peripheral axotomy models in rats (e.g., (Sapunar et al., 2005)) and *Aplysia*
553 (Ungless et al., 2002), and other rodent pain models, such as peripheral inflammation (Qu et al.,
554 2014), chemotherapy (Li et al., 2017), bone cancer (Zheng et al., 2012), and chronic
555 compression of the DRG (Song et al., 2006). Nociceptor hyperexcitability manifested as
556 enhanced repetitive firing (including spontaneous activity), reduced AP threshold, and/or
557 depolarized RMP has been linked to cAMP signaling through PKA, EPAC, or HCN channels in
558 several of these models ((Aley and Levine, 1999; Bavencoffe et al., 2016; Djouhri et al., 2018;
559 Berkey et al., 2020); reviewed by (Li et al., 2019)). In addition, ERK signaling enhances
560 nociceptor function in various pain-related models (e.g. (Obata et al., 2003; Ji et al., 2009;
561 Ferrari et al., 2014; Li et al., 2015; Mihail et al., 2019)). Little is known about how ERK increases
562 nociceptor excitability, although evidence suggests that ERK can directly phosphorylate sodium
563 channel Nav1.7, allowing it to open at more hyperpolarized membrane potentials and perhaps
564 contribute to a more depolarized RMP (Stamboulian et al., 2010). The present study shows that
565 substantial enhancement of the basal activity of AC and ERK activity is produced by modest
566 depolarization of RMP – into the RMP range that occurs naturally in hyperactive nociceptors
567 during persistent pain states. This discovery has important implications. First, it indicates that

568 depolarization of RMP in these states increases the ongoing activity of nociceptors not only by
569 bringing membrane potential closer to AP threshold, but also by increasing the activity of major
570 cell signaling pathways that themselves promote hyperexcitability. Second, the positive
571 feedback between the basal activity of AC and ERK signaling pathways on the one hand and
572 RMP on the other should by itself contribute to the persistence of pain driven by ongoing activity
573 in nociceptors. This positive feedback loop may reinforce persistent hyperexcitable effects
574 mediated by the transcriptional and translational consequences of signaling by AC and ERK
575 (e.g., (Obata et al., 2003; Ferrari et al., 2015)). Moreover, the C-Raf-mediated reduction in
576 sensitivity of AC to Gαi in depolarized nociceptors should further enhance nociceptor activity by
577 reducing suppressive effects of endogenous opioids. Thus, depolarization-dependent C-Raf-
578 ERK and C-Raf-AC signaling should promote nociceptor hyperactivity by multiple, self-
579 reinforcing mechanisms, some of which may reduce the efficacy of clinically applied opioids and
580 cannabinoids. These findings raise important questions about how C-Raf-dependent, MOR-
581 sensitive, nociceptor hyperactivity may contribute to spontaneous pain (Yang et al., 2014), as
582 well as to evoked pain (Sun et al., 2019) and MOR-dependent pathophysiology such as
583 hyperalgesia, Type II hyperalgesic priming, and opioid tolerance (Araldi et al., 2017; Corder et
584 al., 2017; Araldi et al., 2019).

585

Author contributions

A.G.C. and A.B. conducted experiments and collected data. C.W.D and E.T.W. designed the study. All authors contributed to data analyses and writing the manuscript.

590 **References:**

591 Aley K, Levine J (1999) Role of protein kinase A in the maintenance of inflammatory pain. J
592 Neurosci 19:2181-2186.
593 Araldi D, Ferrari LF, Levine JD (2017) Hyperalgesic priming (type II) induced by repeated opioid
594 exposure: maintenance mechanisms. Pain 158:1204-1216.
595 Araldi D, Bogen O, Green PG, Levine JD (2019) Role of Nociceptor Toll-like Receptor 4 (TLR4)
596 in Opioid-Induced Hyperalgesia and Hyperalgesic Priming. J Neurosci 39:6414-6424.
597 Baldassa S, Zippel R, Sturani E (2003) Depolarization-induced signaling to Ras, Rap1 and
598 MAPKs in cortical neurons. Brain Res Mol Brain Res 119:111-122.
599 Barry PH (1994) JPCalc, a software package for calculating liquid junction potential corrections
600 in patch-clamp, intracellular, epithelial and bilayer measurements and for correcting
601 junction potential measurements. J Neurosci Methods 51:107-116.
602 Basso DM, Beattie MS, Bresnahan JC (1995) A sensitive and reliable locomotor rating scale for
603 open field testing in rats. J Neurotrauma 12:1-21.
604 Bavencoffe A, Li Y, Wu Z, Yang Q, Herrera J, Kennedy EJ, Walters ET, Dessauer CW (2016)
605 Persistent Electrical Activity in Primary Nociceptors after Spinal Cord Injury Is
606 Maintained by Scaffolded Adenylyl Cyclase and Protein Kinase A and Is Associated with
607 Altered Adenylyl Cyclase Regulation. J Neurosci 36:1660-1668.
608 Beazely MA, Alan JK, Watts VJ (2005) Protein kinase C and epidermal growth factor stimulation
609 of Raf1 potentiates adenylyl cyclase type 6 activation in intact cells. Molecular
610 pharmacology 67:250-259.
611 Bedi S, Yang Q, Crook R, Du J, Wu Z, Fishman H, Grill R, Carlton S, Walters E (2010) Chronic
612 spontaneous activity generated in the somata of primary nociceptors is associated with
613 pain-related behavior after spinal cord injury. J Neurosci 30:14870-14882.
614 Berkey SC, Herrera JJ, Odem MA, Rahman S, Cheruvu SS, Cheng X, Walters ET, Dessauer
615 CW, Bavencoffe AG (2020) EPAC1 and EPAC2 promote nociceptor hyperactivity

616 associated with chronic pain after spinal cord injury. Neurobiology of pain (Cambridge,
617 Mass) 7:100040.
618 Bryce TN (2018) Opioids should not be prescribed for chronic pain after spinal cord injury.
619 Spinal Cord Ser Cases 4:66.
620 Carlton S, Du J, Tan H, Nesic O, Hargett G, Bopp A, Yamani A, Lin Q, Willis W, Hulsebosch C
621 (2009) Peripheral and central sensitization in remote spinal cord regions contribute to
622 central neuropathic pain after spinal cord injury. Pain 147:265-276.
623 Corbit KC, Trakul N, Eves EM, Diaz B, Marshall M, Rosner MR (2003) Activation of Raf-1
624 signaling by protein kinase C through a mechanism involving Raf kinase inhibitory
625 protein. J Biol Chem 278:13061-13068.
626 Corder G, Tawfik VL, Wang D, Sypek EI, Low SA, Dickinson JR, Sotoudeh C, Clark JD, Barres
627 BA, Bohlen CJ, Scherrer G (2017) Loss of mu opioid receptor signaling in nociceptors,
628 but not microglia, abrogates morphine tolerance without disrupting analgesia. Nat Med
629 23:164-173.
630 de Hoon MJ, Imoto S, Nolan J, Miyano S (2004) Open source clustering software.
631 Bioinformatics (Oxford, England) 20:1453-1454.
632 Dessauer CW, Watts VJ, Ostrom RS, Conti M, Dove S, Seifert R (2017) International Union of
633 Basic and Clinical Pharmacology. CI. Structures and Small Molecule Modulators of
634 Mammalian Adenylyl Cyclases. Pharmacol Rev 69:93-139.
635 Ding Q, Gros R, Gray ID, Taussig R, Ferguson SS, Feldman RD (2004) Raf kinase activation of
636 adenylyl cyclases: isoform-selective regulation. Molecular pharmacology 66:921-928.
637 Djouhri L, Smith T, Ahmeda A, Alotaibi M, Weng X (2018) Hyperpolarization-activated cyclic
638 nucleotide-gated channels contribute to spontaneous activity in L4 C-fiber nociceptors,
639 but not Abeta-non-nociceptors, after axotomy of L5-spinal nerve in the rat in vivo. Pain
640 159:1392-1402.

641 Du X, Hao H, Gigout S, Huang D, Yang Y, Li L, Wang C, Sundt D, Jaffe DB, Zhang H, Gamper
642 N (2014) Control of somatic membrane potential in nociceptive neurons and its
643 implications for peripheral nociceptive transmission. Pain 155:2306-2322.
644 Ferrari LF, Bogen O, Levine JD (2014) Second messengers mediating the expression of
645 neuroplasticity in a model of chronic pain in the rat. J Pain 15:312-320.
646 Ferrari LF, Araldi D, Levine JD (2015) Distinct terminal and cell body mechanisms in the
647 nociceptor mediate hyperalgesic priming. J Neurosci 35:6107-6116.
648 Inder K, Harding A, Plowman SJ, Philips MR, Parton RG, Hancock JF (2008) Activation of the
649 MAPK module from different spatial locations generates distinct system outputs. Mol Biol
650 Cell 19:4776-4784.
651 Isensee J, Diskar M, Waldherr S, Buschow R, Hasenauer J, Prinz A, Allgower F, Herberg FW,
652 Hucho T (2014) Pain modulators regulate the dynamics of PKA-RII phosphorylation in
653 subgroups of sensory neurons. J Cell Sci 127:216-229.
654 Isensee J, Krahe L, Moeller K, Pereira V, Sexton JE, Sun X, Emery E, Wood JN, Hucho T
655 (2017) Synergistic regulation of serotonin and opioid signaling contributes to pain
656 insensitivity in Nav1.7 knockout mice. Sci Signal 10.
657 Isensee J, Kaufholz M, Knape MJ, Hasenauer J, Hammerich H, Gonczarowska-Jorge H, Zahedi
658 RP, Schwede F, Herberg FW, Hucho T (2018) PKA-RII subunit phosphorylation
659 precedes activation by cAMP and regulates activity termination. J Cell Biol 217:2167-
660 2184.
661 Ji RR, Gereau RWt, Malcangio M, Strichartz GR (2009) MAP kinase and pain. Brain Res Rev
662 60:135-148.
663 Kramer JL, Minhas NK, Jutzeler CR, Erskine EL, Liu LJ, Ramer MS (2017) Neuropathic pain
664 following traumatic spinal cord injury: Models, measurement, and mechanisms. J
665 Neurosci Res 95:1295-1306.

666 Leicht DT, Balan V, Kaplun A, Singh-Gupta V, Kaplun L, Dobson M, Tzivion G (2007) Raf
667 kinases: function, regulation and role in human cancer. Biochimica et biophysica acta
668 1773:1196-1212.
669 Li Y, Zhang H, Kosturakis AK, Cassidy RM, Zhang H, Kennamer-Chapman RM, Jawad AB,
670 Colomand CM, Harrison DS, Dougherty PM (2015) MAPK signaling downstream to
671 TLR4 contributes to paclitaxel-induced peripheral neuropathy. Brain Behav Immun
672 49:255-266.
673 Li Y, Tatsui CE, Rhines LD, North RY, Harrison DS, Cassidy RM, Johansson CA, Kosturakis
674 AK, Edwards DD, Zhang H, Dougherty PM (2017) Dorsal root ganglion neurons become
675 hyperexcitable and increase expression of voltage-gated T-type calcium channels
676 (Cav3.2) in paclitaxel-induced peripheral neuropathy. Pain 158:417-429.
677 Li ZH, Cui D, Qiu CJ, Song XJ (2019) Cyclic nucleotide signaling in sensory neuron
678 hyperexcitability and chronic pain after nerve injury. Neurobiol Pain 6:100028.
679 Liu S, Huang Q, He S, Chen Z, Gao X, Ma D, Duan W, Ford N, Yang F, Chen X, Raja SN, Hao
680 D, Guan Y (2019) Dermorphin [D-Arg2, Lys4] (1-4) amide inhibits below-level heat
681 hypersensitivity in mice after contusive thoracic spinal cord injury. Pain 160:2710-2723.
682 McLaughlin KA, Levin M (2018) Bioelectric signaling in regeneration: Mechanisms of ionic
683 controls of growth and form. Dev Biol 433:177-189.
684 Mihail SM, Wangzhou A, Kunjilwar KK, Moy JK, Dussor G, Walters ET, Price TJ (2019) MNK-
685 eIF4E signalling is a highly conserved mechanism for sensory neuron axonal plasticity:
686 evidence from Aplysia californica. Philos Trans R Soc Lond B Biol Sci 374:20190289.
687 Mogil JS (2020) Qualitative sex differences in pain processing: emerging evidence of a biased
688 literature. Nat Rev Neurosci.
689 Obata K, Yamanaka H, Dai Y, Tachibana T, Fukuoka T, Tokunaga A, Yoshikawa H, Noguchi K
690 (2003) Differential activation of extracellular signal-regulated protein kinase in primary

691 afferent neurons regulates brain-derived neurotrophic factor expression after peripheral
692 inflammation and nerve injury. J Neurosci 23:4117-4126.
693 Odem MA, Bavencoffe AG, Cassidy RM, Lopez ER, Tian J, Dessauer CW, Walters ET (2018)
694 Isolated nociceptors reveal multiple specializations for generating irregular ongoing
695 activity associated with ongoing pain. Pain 159:2347-2362.
696 Odem MA, Cassidy RM, Bavencoffe A, Lopez E, Tian J, Wu Z, Dessauer CW, Walters ET
697 (2017) Distinct classes of primary nociceptors show electrophysiological specializations
698 for driving ongoing and evoked pain. Society for Neuroscience Abstract:397.322.
699 Polakiewicz RD, Schieferl SM, Dorner LF, Kansra V, Comb MJ (1998) A mitogen-activated
700 protein kinase pathway is required for mu-opioid receptor desensitization. J Biol Chem
701 273:12402-12406.
702 Qu L, Fan N, Ma C, Wang T, Han L, Fu K, Wang Y, Shimada SG, Dong X, LaMotte RH (2014)
703 Enhanced excitability of MRGPRA3- and MRGPRD-positive nociceptors in a model of
704 inflammatory itch and pain. Brain 137:1039-1050.
705 Ritter DM, Zemel BM, Hala TJ, O'Leary ME, Lepore AC, Covarrubias M (2015) Dysregulation of
706 Kv3.4 channels in dorsal root ganglia following spinal cord injury. J Neurosci 35:1260-
707 1273.
708 Rodriguez-Munoz M, de la Torre-Madrid E, Sanchez-Blazquez P, Garzon J (2011) NO-released
709 zinc supports the simultaneous binding of Raf-1 and PKCgamma cysteine-rich domains
710 to HINT1 protein at the mu-opioid receptor. Antioxid Redox Signal 14:2413-2425.
711 Roederer M (2002) Compensation in flow cytometry. Curr Protoc Cytom Chapter 1:Unit 1 14.
712 Rosen LB, Ginty DD, Weber MJ, Greenberg ME (1994) Membrane depolarization and calcium
713 influx stimulate MEK and MAP kinase via activation of Ras. Neuron 12:1207-1221.
714 Ruland JG, Kirchhofer SB, Klindert S, Bailey CP, Bunemann M (2020) Voltage modulates the
715 effect of mu-receptor activation in a ligand-dependent manner. Br J Pharmacol.

716 Salzer I, Ray S, Schicker K, Boehm S (2019) Nociceptor Signalling through ion Channel
717 Regulation via GPCRs. Int J Mol Sci 20.
718 Sapunar D, Modric-Jednacak K, Grkovic I, Michalkiewicz M, Hogan QH (2005) Effect of
719 peripheral axotomy on pain-related behavior and dorsal root ganglion neurons
720 excitability in NPY transgenic rats. Brain Res 1063:48-58.
721 Song X, Wang Z, Gan Q, Walters E (2006) cAMP and cGMP contribute to sensory neuron
722 hyperexcitability and hyperalgesia in rats with dorsal root ganglia compression. J
723 Neurophysiol 95:479-492.
724 Stamboulian S, Choi JS, Ahn HS, Chang YW, Tyrrell L, Black JA, Waxman SG, Dib-Hajj SD
725 (2010) ERK1/2 mitogen-activated protein kinase phosphorylates sodium channel
726 Na(v)1.7 and alters its gating properties. J Neurosci 30:1637-1647.
727 Strassheim D, Malbon CC (1994) Phosphorylation of Gi alpha 2 attenuates inhibitory adenylyl
728 cyclase in neuroblastoma/glioma hybrid (NG-108-15) cells. J Biol Chem 269:14307-
729 14313.
730 Sun J, Chen SR, Chen H, Pan HL (2019) mu-Opioid receptors in primary sensory neurons are
731 essential for opioid analgesic effect on acute and inflammatory pain and opioid-induced
732 hyperalgesia. J Physiol 597:1661-1675.
733 Tan CM, Kelvin DJ, Litchfield DW, Ferguson SS, Feldman RD (2001) Tyrosine kinase-mediated
734 serine phosphorylation of adenylyl cyclase. Biochemistry 40:1702-1709.
735 Tumati S, Milnes TL, Yamamura HI, Vanderah TW, Roeske WR, Varga EV (2008) Intrathecal
736 Raf-1-selective siRNA attenuates sustained morphine-mediated thermal hyperalgesia.
737 Eur J Pharmacol 601:207-208.
738 Ungless MA, Gasull X, Walters ET (2002) Long-term alteration of S-type potassium current and
739 passive membrane properties in aplysia sensory neurons following axotomy. Journal of
740 neurophysiology 87:2408-2420.

741 Varga EV, Rubenzik M, Grife V, Sugiyama M, Stropova D, Roeske WR, Yamamura HI (2002)
742 Involvement of Raf-1 in chronic delta-opioid receptor agonist-mediated adenylyl cyclase
743 superactivation. Eur J Pharmacol 451:101-102.
744 Vickery ON, Machtens JP, Zachariae U (2016) Membrane potentials regulating GPCRs: insights
745 from experiments and molecular dynamics simulations. Curr Opin Pharmacol 30:44-50.
746 Vierck C (2019) Mechanisms of Below-Level Pain Following Spinal Cord Injury (SCI). J Pain.
747 Wang HB, Zhao B, Zhong YQ, Li KC, Li ZY, Wang Q, Lu YJ, Zhang ZN, He SQ, Zheng HC, Wu
748 SX, Hokfelt TG, Bao L, Zhang X (2010) Coexpression of delta- and mu-opioid receptors
749 in nociceptive sensory neurons. Proc Natl Acad Sci U S A 107:13117-13122.
750 Widerstrom-Noga E (2017) Neuropathic Pain and Spinal Cord Injury: Phenotypes and
751 Pharmacological Management. Drugs 77:967-984.
752 Wu Z, Li L, Xie F, Du J, Zuo Y, Frost JA, Carlton SM, Walters ET, Yang Q (2017) Activation of
753 KCNQ Channels Suppresses Spontaneous Activity in Dorsal Root Ganglion Neurons
754 and Reduces Chronic Pain after Spinal Cord Injury. J Neurotrauma 34:1260-1270.
755 Wu Z, Yang, Q., Crook, R.J., O'Neil, R.G., Walters, E.T. (2013) TRPV1 Channels Make Major
756 Contributions to Behavioral Hypersensitivity and Spontaneous Activity in Nociceptors
757 After Spinal Cord Injury. Pain 154:2130-2141.
758 Yang Q, Wu Z, Hadden JK, Odem MA, Zuo Y, Crook RJ, Frost JA, Walters ET (2014) Persistent
759 pain after spinal cord injury is maintained by primary afferent activity. J Neurosci
760 34:10765-10769.
761 Zhang L, Loh HH, Law PY (2013) A novel noncanonical signaling pathway for the mu-opioid
762 receptor. Molecular pharmacology 84:844-853.
763 Zhang X, Bao L, Li S (2015) Opioid receptor trafficking and interaction in nociceptors. British
764 journal of pharmacology 172:364-374.
765 Zheng Q, Fang D, Cai J, Wan Y, Han JS, Xing GG (2012) Enhanced excitability of small dorsal
766 root ganglion neurons in rats with bone cancer pain. Mol Pain 8:24.

767 **Figure Legends**

768 **Fig. 1. SCI reduces the effect of MOR agonist DAMGO on cAMP signaling. *A,***
769 Phosphorylation of PKA-RII (S99) is used as a surrogate measurement of cAMP production in
770 response to forskolin (Fsk) activation of AC and inhibition by the Gαi/o-coupled Mu opioid
771 receptor (MOR) agonist, DAMGO. ***B,*** DAMGO inhibition of Fsk responses in Control group (Ctrl,
772 white boxes, pooled Naïve and Sham groups) and SCI group (Fsk 3 μM, DAMGO 0.3 μM, 5
773 min). PKA-pRII levels are normalized to the baseline of the unstimulated condition in each case.
774 Ctrl n= 9, SCI n=7, compared via 2-way ANOVA, followed by Sidak's multiple comparisons test;
775 significant *p* values are indicated on the graph. The box-whisker plot indicates the median,
776 mean (+), quartiles, and range (min-max) of the data. ***C,*** Dose-response curves for DAMGO
777 inhibition of Fsk responses (Fsk 3 μM) in Control group (black line) and SCI (red) DRG cultures.
778 PKA-pRII data was normalized to the Fsk response in absence of DAMGO after baseline (BL)
779 subtraction [Y_{Norm}= (Y-BL)/(Fsk_{Max}-BL)]. IC_{50}: Ctrl= 0.047 μM (n=17-22), SCI=0.15 μM (n=15-17),
780 difference between groups tested by 2-way ANOVA, followed by Sidak's test. *p<0.05, **p<0.01,
781 ***p<0.001, ****p<0.0001. Data are presented as mean±SEM. ***D,*** IC_{50} values from individual
782 DAMGO dose-response curves between Control and SCI cultures; $p=2x10^{-5}$, Mann Whitney
783 test, Ctrl n=20, SCI n=16. In the control column, IC_{50} values from Sham controls are denoted by
784 blue empty circles, while naïve controls are represented by black circles. The box-whisker plot
785 indicates the median, mean (+), quartiles, and range (min-max) of the data. Detailed statistical
786 information provided in table 1.

787 **Fig. 2. Cluster analysis of DRG neurons. *A,*** 3D representation of DRG neurons in culture
788 (7,638 neurons) using Area (X), CGRP (Y) and IB4 (Z) values as spatial coordinates. Different
789 colors represent the 7 different clusters identified K-medians cluster analysis and plotted based
790 on X,Y,Z coordinates. Neurons from 2 different $IB4^+$ clusters are represented as a single group.
791 ***B,*** Representative experiment showing the neuronal subgroup specificity of PKA-pRII responses

792 to Fsk in cultured neurons from a naive animal. Dot color saturation is proportional to the
793 intensity of PKA-pRII fluorescent values, with darker colors indicating stronger PKA-pRII signals
794 (n>2,000 neurons per condition) ***C,*** Representative examples of DRG neurons arranged
795 according to the identified clusters in ***A***. GGRP (white), IB4 (red), and soma size (indicated by
796 green outline of cell membrane based on PGP9.5). Clusters include N (neurons negative for IB4
797 and CGRP, with small soma size), CGRP, IB-CG (weak staining for both IB4 and CGRP), IB4, L
798 and XL (large and extra-large soma size). Scale bar = 25 µm. ***D,*** Relative mean cluster size in
799 the total neuronal population for naive and SCI cultures. Colors correspond to clusters in panel
800 ***A*** and ***C***; light and dark green represent weak and strong IB4 staining clusters, respectively. No
801 significant differences in relative cluster size were found between naive and SCI groups.
802 (p>0.99, n=3 per group, 2-way ANOVA, followed by Sidak's test). ***E-F,*** Fsk responses and
803 DAMGO effects in specific neuronal clusters for naive (E) and SCI (F) cultures. n=3 per group,
804 DAMGO effects per cluster tested via paired *t* test. The % DAMGO inhibition over the control
805 Fsk response is indicated for each group. # (red) denotes significance difference in DAMGO
806 effects comparing IB-CG and $IB4^+$ clusters from naïve (E) and SCI (F) n=3, unpaired *t* test.
807 Detailed statistical information provided in table 1.

808 **Fig. 3. Acute depolarization activates ERK and reduces DAMGO effects on cAMP.** ***A***,
809 Resting membrane potential (RMP) for Naive (black) and SCI (red) small to medium-sized DRG
810 neurons was measured upon successive perfusions (30 sec) of increasing extracellular K^+
811 concentration, $[K^+]_e$. RMP at each $[K^+]_e$ was measured when steady-state was reached. n=11,
812 *p=0.039, **p=0.0081, 2-way ANOVA with Sidak's test. ***B, C,*** Concentration-response curves for
813 pERK (***B***) and PKA-pRII (***C***) to increased $[K^+]_e$. Neurons were exposed to media with indicated
814 $[K^+]_e$ for 5 min; *B*, Naive n=5-7, SCI n=5 per data point, *C,* Naïve n=*5*, SCI n=5-7 per data point.
815 2-way ANOVA followed by Sidak's test. ***D,*** pERK responses to 18 mM $[K^+]_e$ (5 min) for $IB4^+$ and
816 $IB4^-$ neuronal subpopulations in naive and SCI DRG neurons; Naïve, SCI n=3, p=0.027, 2-way

817 ANOVA followed by Sidak's test. ***E,*** K^+-induced depolarization decreases DAMGO responses in
818 naive DRG neurons. Neurons were exposed to either control media (5 mM $[K^+]_e$) or 15 mM $[K^+]_e$
819 media during Fsk ± DAMGO (Dm) stimulation (Fsk=3 μM, DAMGO=1 μM, 5 min); n=6, Ctrl
820 *p*=0.041, Fsk+DAMGO *p*=0.0015, 2-way ANOVA, followed by Sidak's test. The box-whisker plot
821 indicates the median, mean (+), quartiles, and range (min-max) of the data. ***F,*** Dose-response
822 curves of DAMGO inhibition of Fsk responses in naive DRG neurons under control conditions
823 (black) or 15 mM $[K^+]_e$ (blue). IC_{50} Control=0.051 μM; IC_{50} K^+15=0.075 μM; Control n=9-19, K^+15
824 n=4-12 per data point. Data compared by 2-way ANOVA, followed by Sidak's test, ****p<0.0001.
825 ***G,*** Dose-response curves of morphine inhibition of Fsk responses in naive DRG neurons with
826 control or 15 mM $[K^+]_e$. Control IC_{50}=0.021 μM, K^+15 IC_{50}=0.16 μM; Control n=3-5, K^+15 n=4-5
827 per data point , 2-way ANOVA. Detailed statistical information provided in table 1.

828 **Fig. 4. Inhibition of C-Raf partially restores opioid sensitivity after depolarization. *A,***
829 Inhibition of 15 mM $[K^+]_e$ effects on DAMGO responses. DRG neurons were preincubated with
830 inhibitors of Src (saracatinib, 10 μM), PKC (sotrastaurin, 1 μM), PKA (H89, 10 μM), C/B-Raf
831 (RAF709, 10 μM), C-Raf (GW5074, 3 μM) or MEK1/2 (UO126, 10 μM) for 30 min and then
832 stimulated with Fsk (3 μM) ± DAMGO (0.1 μM) in control media or 15 mM $[K^+]_e$ (K^+15; 5 min).
833 Effects are reported as inhibition of the control Fsk response (1.0). Drug effects were compared
834 against the Control-DAMGO inhibition (*) or GDNF-DAMGO inhibition (#) via 1-Way ANOVA,
835 followed by Dunnett's test. Significance and n numbers are reported on each bar. **p*<0.05;
836 ***p*<0.01, ****p*<0.001, *****p*<0.0001, ## *p*< 0.01. ***B,*** C-Raf inhibition restores DAMGO IC_{50} in 15
837 mM $[K^+]_e$, but has no effect on DAMGO efficacy (E_{max}). GW5074 (10 μM) was applied 30 min
838 before simultaneous addition of K+15 mM, Fsk (3 mM), and DAMGO for 5 min. Per data point,
839 Control n=10-21, K^+15 n=6-22, K^+15+GW5074=3-10, Ctrl+GW5074=3-11. Treatment effects
840 were compared using 2-Way ANOVA followed by Tukey's multiple comparisons test. Individual
841 data point comparisons using Sidak's test can be found in Table 1. ***C, D***, Quantification of

842 individual IC_{50} (*C*) and E_{max} (*D*) values of DAMGO dose-response curves as described in *B*. For
843 *C,* Ctrl n=13, K^+15(-) n=10, K^+15(GW) n=4. For *D,* Ctrl n=14, K^+15(-) n=10, K^+15(GW) n=4 Data
844 were compared using 1-Way ANOVA, followed by Tukey's test. The box-whisker plot indicates
845 the median, mean (+), quartiles, and range (min-max) of the data. Detailed statistical
846 information provided in table 1.

847 **Fig. 5. Depolarization induces C-Raf activation and relief of RKIP inhibition in IB4$^+$**
848 **neurons. A,** C-Raf activity is promoted by phosphorylation (S338). C-Raf inhibition is relieved
849 upon phosphorylation of RKIP(S153). ***B,*** Phosphorylation of C-Raf (S338) and RKIP (S153) in
850 response to increasing $[K^+]_e$ (5 min stimulation). pC-Raf_{S338} n=3-7, $pRKIP_{S153}$ n=3. ***C,***
851 Phosphorylation of C-Raf (S338) with 15 mM $[K^+]_e$ in naive and SCI DRG neurons; Naïve n=6,
852 SCI n=5. Data compared via unpaired *t* test. The box-whisker plot indicates the median, mean
853 (+), quartiles, and range (min-max) of the data. ***D, E***, Quantification of pC-Raf_{s338} (*D*, n=4) and
854 $pRKIP_{S153}$ (*E*, n=3) phosphorylation in naïve neurons in response to 5 min 15 mM $[K^+]_e$ between
855 different neuronal subpopulations (cluster analysis performed as Fig. *2*). Differences in cluster
856 responses determined via 1-Way ANOVA, followed by Tukey's test. pC-Raf_{S338} and $pRKIP_{S153}$
857 responses have been normalized to control baselines for each cluster. *p* values in the figure
858 correspond to the comparison against IB4. Detailed statistical information provided in Table 1.
859 ***F,*** C-Raf and RKIP phosphorylation in control and 15 mM $[K^+]_e$, shown as coordinates of
860 nociceptor Area (X), CGRP (Y) and IB4 (Z) intensity. Dot color saturation is proportional to the
861 intensity of fluorescent signal, with darker colors indicating stronger signals; pRKIP: n>1,000
862 neurons; pC-Raf: n>3,200 neurons. ***G,*** Examples of pC-Raf_{S338} responses to depolarization (5
863 min,15 mM $[K^+]_e$). 10x magnification, scale bar =25 μm.

864 **Fig. 6. Effects of depolarization and C-Raf activation on HEK-293_{MOR} cells. *A,*** DAMGO
865 dose-response curves in control conditions ($[K^+]_e$ 5 mM, serum-starved, black empty circles),
866 $[K^+]_e$ 15 mM (blue circles), C-Raf-CTH overexpression (Raf-CTH; purple triangles, dotted line),

867 serum treatment (not starved, red squares), or serum in presence of 3 μM the C-Raf inhibitor
868 GW5074 (Ser+GW; orange circles, dotted line). Control n=7-9, K^+15 n=3, Serum n=3-11, Raf-
869 CTH n=6, Ser+GW n=7-8 per data point. Treatment effects were compared via 2-Way ANOVA,
870 followed by Sidak's test. *p<0.05, ** p<0.01, ***p<0.001, ****p<0.0001. Significance symbols:
871 *[Ctrl vs. Raf-CTH], ^[Ctrl vs. Serum], ˅[Serum vs. Ser+GW]. ***B,C,*** Effects of the different
872 treatments used in ***A,*** on DAMGO IC_{50} (B) and E_{max} (C). 50 mM K^+ not shown in ***A***. For *B*: Ctrl
873 n=9, K^+15 n=3, K^+50 n=3, Ser n=9, Raf-CTH n=6, Ser+GW n=7. For *C*: Ctrl n=9, K^+15 n=3, K^+50
874 n=3, Ser n=8, Raf-CTH n=6, Ser+GW n=7. Treatment effects compared via 1-Way ANOVA
875 followed by Dunnett's test. The box-whisker plot indicates the median, mean (+), quartiles, and
876 range (min-max) of the data. Detailed statistical information provided in table 1.

877

878 **Fig. 7. Inhibition of C-Raf fully restores opioid sensitivity and reverses hyperexcitability**
879 **after depolarization.** ***A,*** DAMGO inhibition of Fsk responses in SCI cultured neurons pretreated
880 for 30 min with vehicle (DMSO ≤0.1%), GW5074 (3 μM) or retigabine (10 μM), followed by 5 min
881 stimulation with Fsk (3 μM) +/- indicated concentrations of DAMGO. Vehicle n=11, GW5074 n=
882 7-8, Retigabine n=4. Treatment effects compared via 2-Way ANOVA, followed by Sidak's test.
883 *p<0.05, **p<0.01. Significance symbols: *****[Vehicle vs. Retigabine], **^**[Vehicle vs. GW5074]. ***B,***
884 IC_{50} values from individual DAMGO dose-response curves for SCI groups treated as in ***A***. Veh
885 n=10, GW n=8, Ret n=4. Treatment effects compared using 1-Way ANOVA, followed by
886 Dunnett's test. The box-whisker plot indicates the median, mean (+), quartiles, and range (min-
887 max) of the data. ***C,*** Representative traces of current clamp recordings (I = 0) of sensory
888 neurons isolated from Naive and SCI groups pretreated (30 min) with vehicle (DMSO 0.03%),
889 C-Raf inhibitor (GW5074, 3 μM) or MEK inhibitor (UO126, 3 μM μM). Action potentials are
890 clipped at 0 mV so that subthreshold DSFs are more visible. ***D,*** A selective C-Raf inhibitor
891 (GW5074) and MEK inhibitor (UO126) decrease the incidence (%) of neurons exhibiting

892 ongoing firing at RMP (spontaneous activity) or when held at -45 mV. Comparisons of active
893 neuron incidence by Fisher's exact test. n numbers and *p* values are indicated over each bar.
894 For multiple comparisons, Bonferroni correction was applied and significance levels were as
895 follows: * p < 0.025, ** p , 0.005, *** p < 0.0005. ***E,*** Inhibition of C-Raf or MEK by GW5074 or
896 UO126, respectively, hyperpolarizes RMP. The effects of C-Raf and MEK inhibitors on RMP
897 were compared with Brown-Forsythe and Welch ANOVA, followed by Dunnett's test (*p*=0.011
898 for GW5074 and *p*=0.035 for UO126). ***F,*** Reduction of DSF amplitudes by GW5074 and UO126.
899 Mean DSF amplitudes trended lower when recorded at RMP (*p*=0.055 for each inhibitor) and
900 were significantly lower at -45 mV (*p*=0.033 for GW5074 and *p*=0.013 for UO126). 1-way
901 ANOVA followed by Holm-Sidak's test at RMP and Kruskal-Wallis with Dunn's multiple
902 comparison test at -45 mV. DSF, depolarizing spontaneous fluctuation; MP, membrane
903 potential; RMP, resting membrane potential. Detailed statistical information provided in table 1.

904 **Fig. 8. Model of depolarization-dependent, C-Raf-mediated self-reinforcing mechanisms**
905 **driving nociceptor hyperexcitability and reduced opioid responses after SCI.**
906 Depolarization of nociceptors (ΔVm) induced by SCI enhances C-Raf activity in IB4$^+$ neurons
907 via direct phosphorylation of C-Raf and relief from RKIP inhibition. Active C-Raf promotes
908 hyperexcitability via two different mechanisms acting in parallel. (1) Activation of the MEK-ERK
909 cascade by C-Raf has direct effects on RMP and neuronal excitability. (2) Phosphorylation of
910 AC5/6 by C-Raf reduces the inhibitory effects of Gαi on cAMP generation by AC and
911 downstream PKA/EPAC signaling, which also regulate nociceptor hyperexcitability and RMP.
912 The combined effects of MAPK and cAMP signaling on RMP and hyperexcitability set up
913 positive feedback that maintains ongoing/spontaneous activity in nociceptors while also limiting
914 the effectiveness of opioids.

915

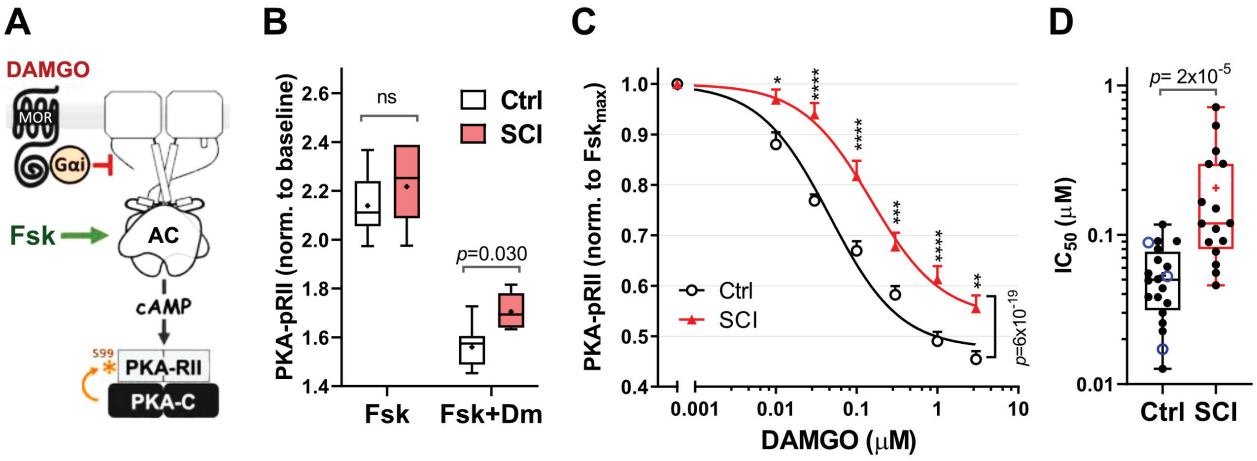

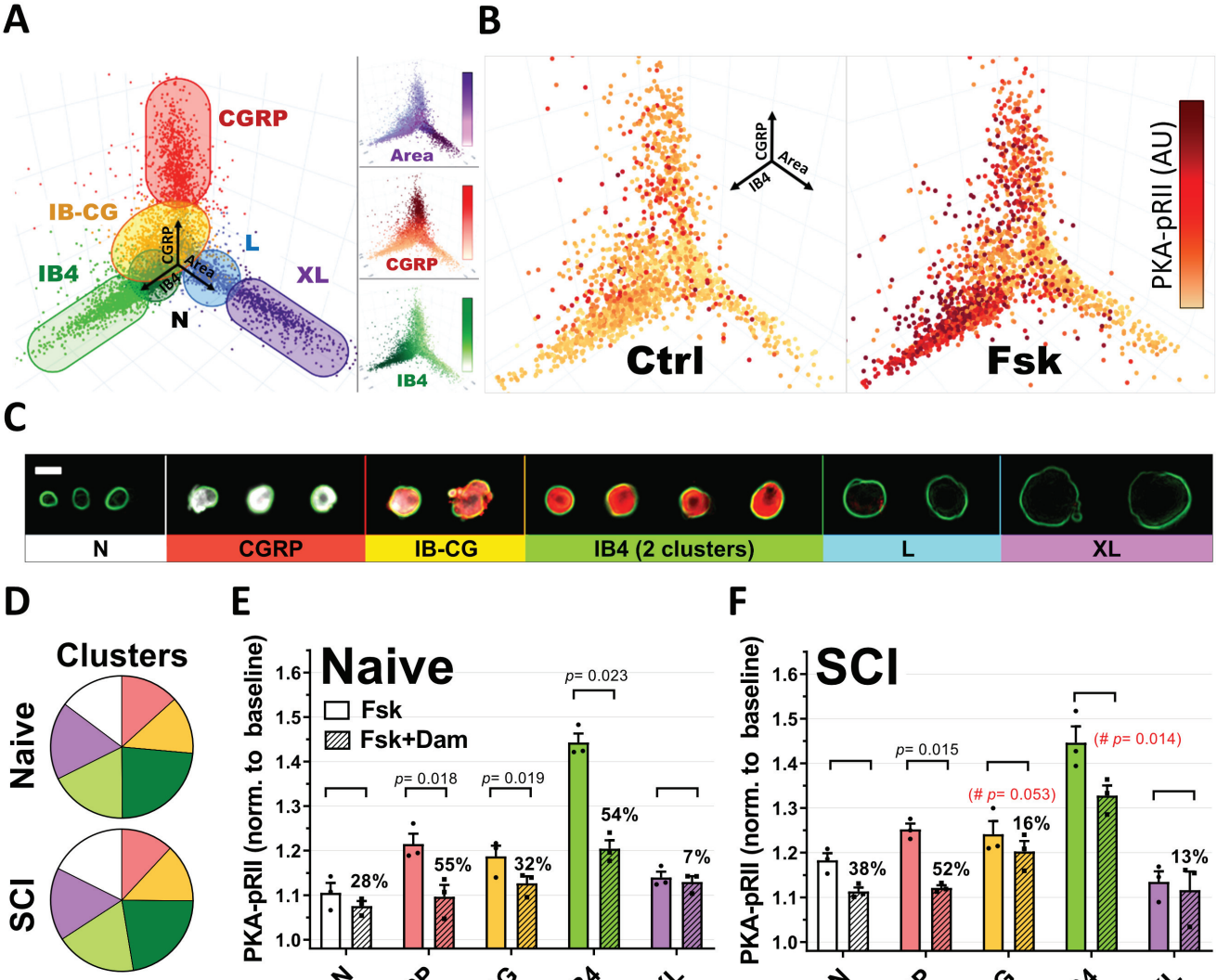

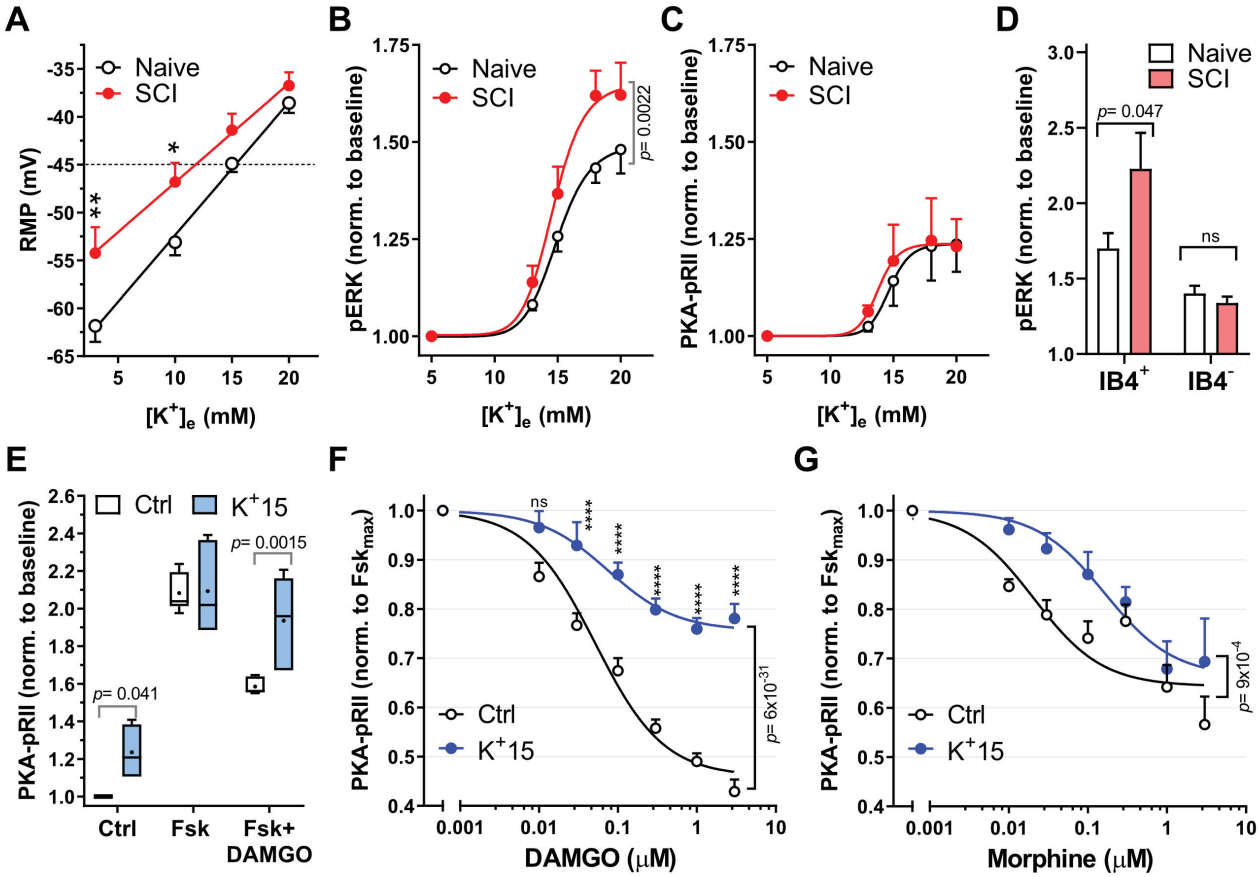

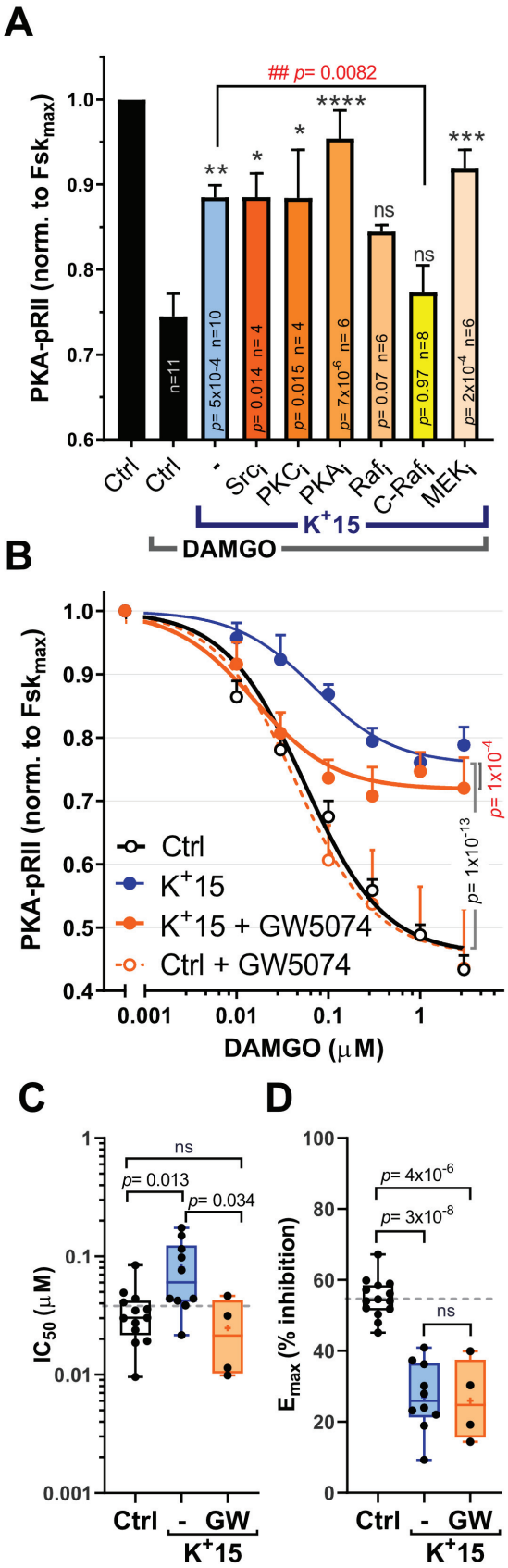

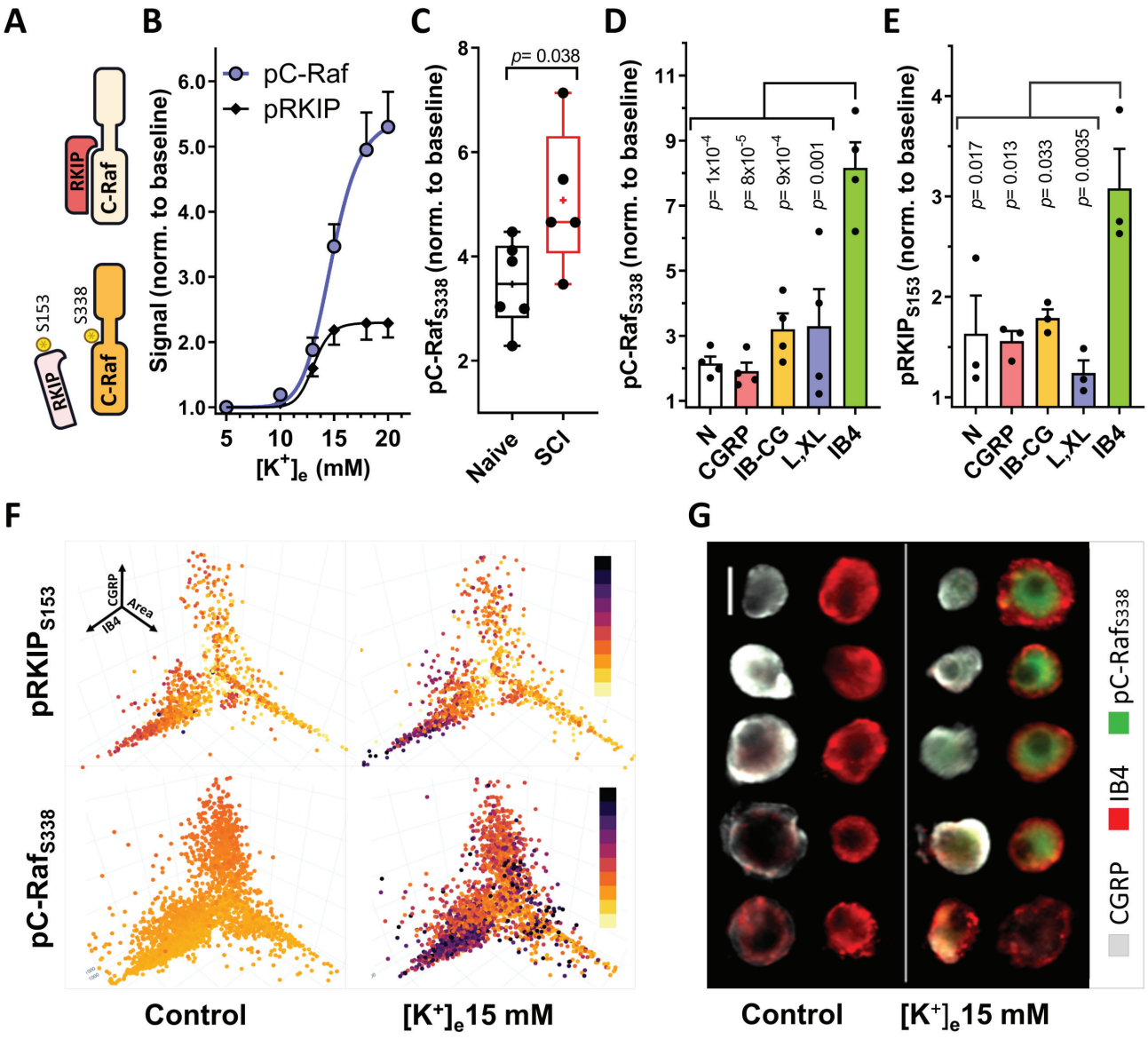

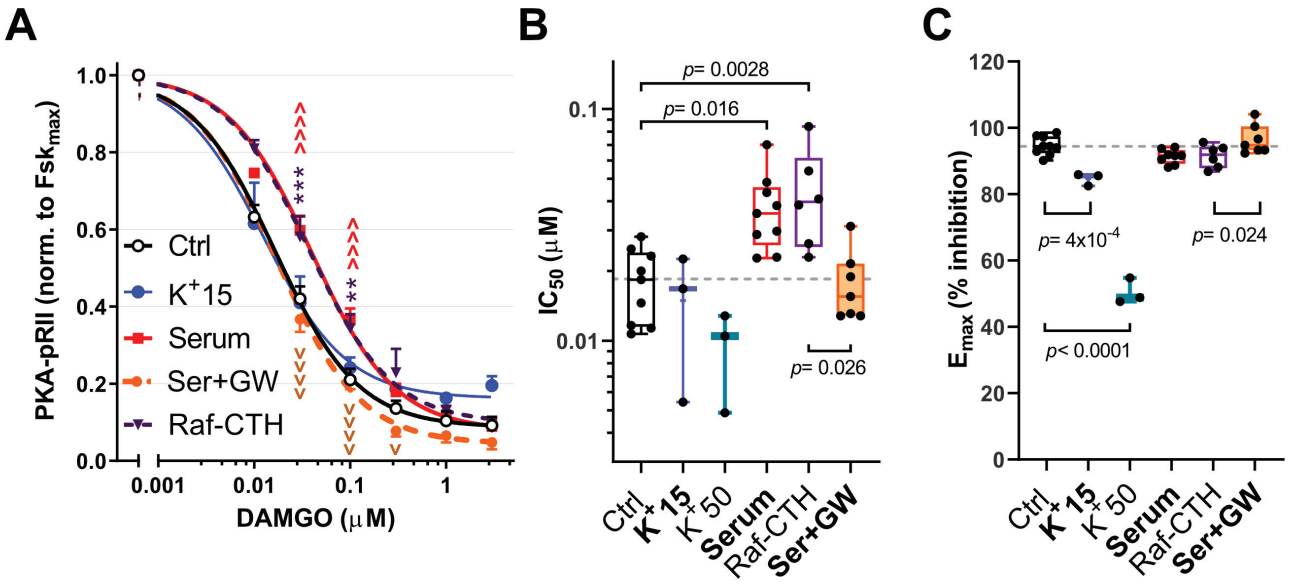

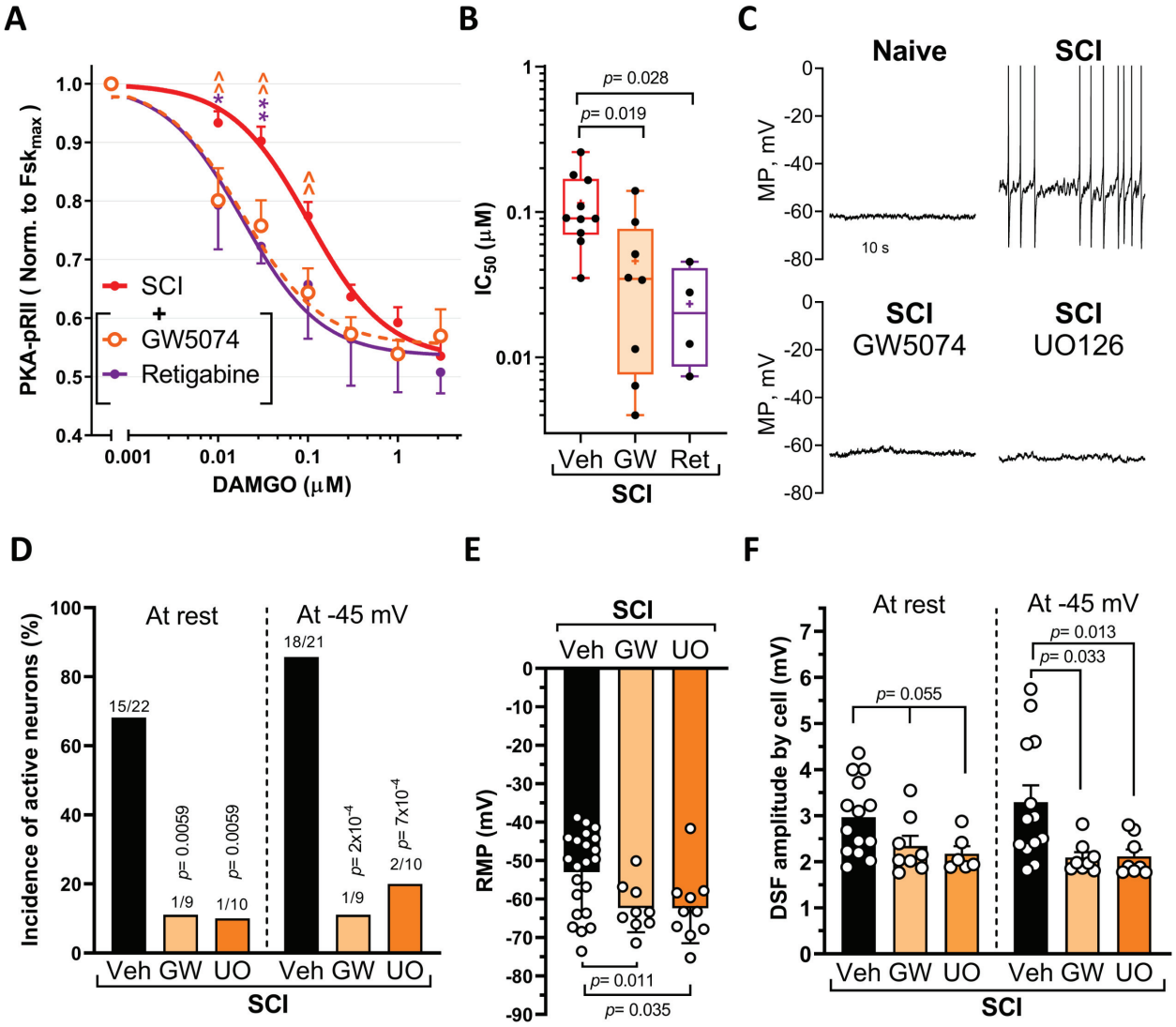

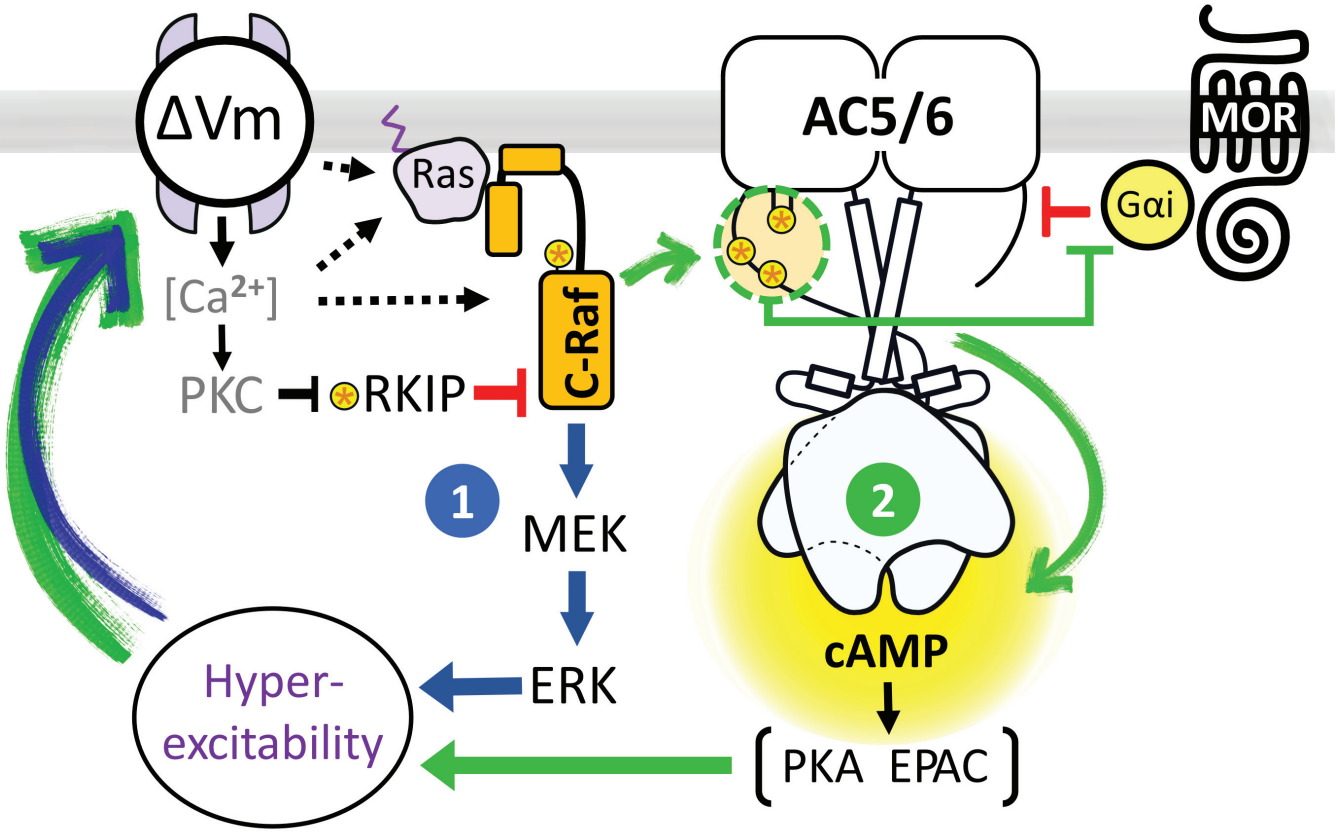

Table 1. Statistical analysis per figure.

Fig.	Test	Post hoc comparison
1B	2-way ANOVA Interaction $F_{(1, 28)}$ =0.71 p=0.41 DAMGO effect $F_{(1, 28)}$ =188 p=6x10^{-14} SCI effect $F_{(1, 28)}$ =7.91 p=0.0089	Sidak's multiple comparisons test *p=0.03 at Fsk+Dm
1C	2-way ANOVA Interaction $F_{(1, 246)}$ =3.89 p=0.001 DAMGO effect $F_{(1, 246)}$ =178.65 p=1x10^{-86} SCI effect $F_{(1, 246)}$ =93.4 p=6x10^{-19}	Sidak's multiple comparisons test. At DAMGO 0.01 µM *p=0.032; 0.03 µM ****p=2x10^{-8}; 0.1 µM ****p=1x10^{-6}; 0.3 µM **p=0.0048; 1 µM ***p=1x10^{-4}; 3 µM **p=0.0045.
1D	Mann Whitney test U=34, p=2x10^{-5}	
2D	2-way ANOVA Interaction $F_{(5, 24)}$ =0.40 p=0.84 Between clusters $F_{(5, 24)}$ =8.43 p=1x10^{-4} Naïve vs. SCI $F_{(1, 24)}$ =6x10^{-5} p=0.99	Sidak's multiple comparisons test
2E	Paired t test (two tailed), DAMGO effect Naïve: CGRP ($t_{(2)=}$7.34, p=0.081), IB-CG ($t_{(2)=}$7.23, p=0.019), IB4 ($t_{(2)=}$6.52, p=0.023)	
2F	Paired t test (DAMGO Effect) 2F_SCI: CGRP ($t_{(2)=}$8.17, p=0.015)	
2F*	Unpaired t test (SCI effect) [Fsk +DAMGO] Naïve vs. SCI: IB4 ($t_{(4)=}$4.15, p=0.014).	
3A	2-way RM ANOVA Interaction $F_{(3, 60)}$ =3.67 p=0.017 K^+ effect $F_{(3, 60)}$ =165 p=6.19x10^{-2} SCI effect $F_{(1, 20)}$ =5.4 p=0.031	Sidak's multiple comparisons test **p=0.0081 at 3 mM; *p=0.039 at 10 mM.
3B	2-way ANOVA Interaction $F_{(4, 46)}$ =1.14 p=0.35 K^+ effect $F_{(4, 46)}$ =53.51 p=1x10^{-17} SCI effect $F_{(1, 46)}$ =10.51 p=0.0022	Sidak's multiple comparisons test

3C	2-way ANOVA			Sidak's multiple comparisons test
	Interaction	$F_{(4, 46)}$ =0.079	p=0.99	
	K^+ effect	$F_{(4, 46)}$ =6.4	p=4x10^{-4}	
	SCI effect	$F_{(1, 46)}$ =0.25	p=0.62	
3D	2-way ANOVA			Sidak's multiple comparisons test (Naïve vs. SCI)
	Interaction	$F_{(1, 8)}$ =4.87	p=0.058	IB4$^+$: *p=0.047
	IB4 effect	$F_{(1, 8)}$ =19.55	p=0.0022	
	SCI effect	$F_{(1, 8)}$ =3	p=0.12	
3E	2-way ANOVA			Sidak's multiple comparisons test
	Interaction	$F_{(2, 30)}$ =3.7	p=0.036	[Ctrl]: p=0.041; [Fsk+DAMGO]: p=0.0015.
	Stimuli effect	$F_{(2, 30)}$ =120.2	p=5x10^{-15}	
	K^+ effect	$F_{(1, 30)}$ =14.63	p=6x10^{-4}	
3F	2-way ANOVA			Sidak's multiple comparisons test
	Interaction	$F_{(6, 158)}$ =13.35	p=3x10^{-12}	At DAMGO 0.03 µM ****p=4x10^{-5}; 0.1 µM ****p=4x10^{-8}; 0.3 µM ****p=1x10^{-12}; 1 µM ****p=2x10^{-15}; 3 µM ****p< 0.0001.
	DAMGO effect	$F_{(6, 158)}$ =90.18	p=2x10^{-48}	
	K^+ effect	$F_{(1, 158)}$ =211.8	p=6x10^{-31}	
3G	2-way ANOVA			Sidak's multiple comparisons test
	Interaction	$F_{(6, 49)}$ =13.35	p=0.55	
	DAMGO effect	$F_{(6, 49)}$ =90.18	p=1x10^{-11}	
	K^+ effect	$F_{(1, 49)}$ =211.8	p=9x10^{-4}	
4A	1-Way ANOVA			Sidak's multiple comparisons test (vs. [Ctrl] group).
	$F_{(7, 47)}$ =7.54, p=4x10^{-6}			[-]: ***p=5x10^{-4}, [Src$_i$]: *p=0.014, [PKC$_i$] *p=0.015, [PKA$_i$] ****p=7x10^{-6}, [MEK$_i$] ***p=2x10^{-4}.
4A#	1-Way ANOVA			Dunnett's multiple comparisons test (vs. [-] group).
	$F_{(6, 37)}$ =7.54, p=8x10^{-4}			C-Raf$_i$ ##p=0.0082.
4B	2-way ANOVA			Tukey's multiple comparisons test.
	Interaction	$F_{(15, 266)}$ =11.2	p=5x10^{-21}	[Ctrl] vs. [K^+15]: p= 1x10^{-13}, [Ctrl] vs. [K^+15+GW5074]: p=2x10^{-13}, [K^+15] vs. [K^+15+GW5074]: p=1x10^{-4}.
	DAMGO effect	$F_{(5, 266)}$ =191.4	p=6x10^{-86}	
	Treatment effect	$F_{(3, 266)}$ =133.3	p=1x10^{-52}	
4B	2-way ANOVA			Sidak's multiple comparisons test (Ctrl + GW5074 excluded)
	Interaction	$F_{(10, 229)}$ =13.25	p=3x10^{-18}	[Ctrl] vs. [K^+15]: 0.03 µM p=3x10^{-5}; 0.1 µM p=1x10^{-12}; 0.3 µM p=4x10^{-15}; 1 µM p< 0.0001; 3 µM p< 0.0001.
	DAMGO effect	$F_{(5, 229)}$ =118.64	p=2x10^{-61}	
	Treatment effect	$F_{(2, 229)}$ =163.3	p=9x10^{-45}	[K^+15] vs. [K^+15+GW5074]: 0.1 µM p=5x10$^{-5.}$
				[Ctrl] vs. [K^+15+GW5074]: 0.3 µM p=0.0015; 1 µM p=6 x10^{-15}; 3 µM p=7x10^{-8}.
4C	1-Way ANOVA			Tukey's multiple comparisons test
	$F_{(2, 24)}$ =6.07, p=0.0074			

		Ctrl vs. K^+15(-): p=0.013; K^+15(-) vs. K^+(GW): p=0.034
4D	1-Way ANOVA $F_{(2, 25)}$ =42.94, p=8x10^{-9}	Tukey's multiple comparisons test Ctrl vs. K^+15(-): 3x10^{-8}; Ctrl vs. K^+(GW): 4x10^{-6}
5C	Unpaired t test (two-tailed) $t_{(9)}$=3.57, p=0.038.	
5D	1-way ANOVA $F_{(4, 15)}$ =14.31, p=5x10^{-6}	Tukey's multiple comparisons test N vs. IB4: p=1x10^{-4}, CGRP vs. IB4: p=8x10^{-5}, IB-CG vs. IB4: p=9x10^{-4}, L,XL vs. IB4: p=0.001
5E	1-way ANOVA $F_{(4, 10)}$ =7.68, p=0.0044	Tukey's multiple comparisons test N vs. IB4: p=0.017, CGRP vs. IB4: p=0.013, IB-CG vs. IB4: p=0.033, L,XL vs. IB4: p=0.0035
6A	2-way ANOVA (0.01 µM point excluded) Interaction $F_{(20, 185)}$ =3.28 p=1x10^{-5} DAMGO effect $F_{(5, 185)}$ =669.2 p=2x10^{-116} Treatment effect $F_{(4, 185)}$ =15.94 p=3x10^{-11}	Sidak's multiple comparisons test [Ctrl] vs. [Serum]: 0.03 µM ^^^^p=4x10^{-6}; 0.1 µM ^^^p=4x10^{-5}; [Ctrl] vs.[Raf-CTH]: 0.03 µM ***p=5x10^{-4}; 0.1 µM **p=0.0062; 0.3 µM *p=0.024 [Serum] vs. [Ser+GW]: 0.03 µM ^{vvvv} p=1x10^{-8}; 0.1 µM ^{vvvv}p=8x10^{-5}; 0.3 µM ^{v}p=0.043
6B	1-Way ANOVA $F_{(5, 31)}$ =6.72, p=2x10^{-4}	Sidak's multiple comparisons test Ctrl vs. Serum: p=0.016, Ctrl vs. Raf-CTH: p=0.0028, Serum vs. Ser+GW: p=0.026
6C	1-Way ANOVA $F_{(5, 30)}$ =103.51, p=6x10^{-18}	Sidak's multiple comparisons test Ctrl vs. K^+15: p=4x10^{-4}, Ctrl vs. K+50: p< 0.0001, Serum vs. Ser+GW: p=0.024
7A	2-Way ANOVA Interaction $F_{(14, 158)}$ =1.79 p=0.044 DAMGO effect $F_{(7, 158)}$ =89.08 p=1x10^{-51} Treatment effect $F_{(2,158)}$ =12.99 p=6x10^{-6}	Sidak's multiple comparisons test (Treatment effects) SCI vs. GW5074: p=9x10^{-5}, SCI vs. Retigabine: p=1x10^{-4}
7A	2-Way ANOVA Interaction $F_{(14, 158)}$ =1.79 p=0.044 DAMGO effect $F_{(7, 158)}$ =89.08 p=1x10^{-51} Treatment effect $F_{(2,158)}$ =12.99 p=6x10^{-6}	Sidak's multiple comparisons test (Individual data points) SCI vs. GW5074: 0.01 µM ^^p=0.0054; 0.03 µM ^^p=0.0034; 0.1 µM ^^p=0.0087 SCI vs. Retigabine: 0.01 µM *p=0.022; 0.03 µM **p=0.0025
7B	1-Way ANOVA	Dunnett's multiple comparisons test

	$F_{(2, 19)}$=5.69, p=0.012	Veh vs. GW: p=0.028, Veh vs. Ret: p=0.019
7D	Fisher's exact test	Bonferroni correction for two comparisons, significance levels: * p < 0.025, ** p , 0.005, *** p < 0.0005 <u>At rest</u> Veh vs GW: * p =0.0059 Veh vs UO126: * p =0.0059 <u>At -45 mV</u> Veh vs GW: *** p =0.0002 Veh vs UO126: ** p =0.0007
7E	Brown-Forsythe and Welch ANOVA tests, respectively: $F_{(2, 30.80)}$ =6.18, p =0.0055 $W_{(2, 20.56)}$ =5.377, p =0.0132	Dunnett's multiple comparisons test Veh vs GW: p =0.011 Veh vs UO126: p =0.035
7F	At rest: 1-Way ANOVA $F_{(2, 25)}$ =3.616, p =0.0418 At -45 mV: Kruskal-Wallis test p =0.0086	<u>At rest</u>: Holm-Sidak's multiple comparison test Veh vs GW: p =0.055 Veh vs UO126: p =0.055 <u>At -45 mV</u>: Dunn's multiple comparison test Veh vs GW: p =0.034 Veh vs UO126: p =0.013